

1 **Linking shifts in bacterial community with changes in dissolved organic matter pool in**  
2 **a tropical lake**

3

4 Marcelo P. Ávila<sup>1</sup>, Luciana P. M. Brandão<sup>1</sup>, Ludmila S. Brighenti<sup>1</sup>, Denise Tonetta<sup>1</sup>, Mariana  
5 P. Reis<sup>1</sup>, Peter A. Staehr<sup>2</sup>, Eero Asmala<sup>2,3</sup>, André M. Amado<sup>4</sup>, Francisco A. R. Barbosa<sup>1</sup>, José  
6 F. Bezerra-Neto<sup>1</sup>, Andréa M. A. Nascimento<sup>1\*</sup>

7

8 <sup>1</sup>Departamento de Biologia Geral, Instituto de Ciências Biológicas, Universidade Federal de  
9 Minas Gerais, Belo Horizonte, MG 31270-901, Brazil

10 <sup>2</sup>Department of Bioscience, Aarhus University, Frederiksborgvej 399, Box 358, 4000  
11 Roskilde, Denmark

12 <sup>3</sup>Tvärminne Zoological Station, University of Helsinki, J.A. Palménin tie 260, 10900 Hanko,  
13 Finland

14 <sup>4</sup>Limnology Laboratory, Department of Oceanography and Limnology, Universidade Federal  
15 do Rio Grande do Norte, Rio Grande do Norte, Brazil,

16

17 \*Corresponding author: Andréa M. A. Nascimento. Institutional address: Avenida Antônio  
18 Carlos 6627, 31270-901, Belo Horizonte, MG, Brazil. Phone: +55 31 3409 2588; fax: +55 31  
19 3409 2567; e-mail: amaral@ufmg.br

20

21

22

23

24

25

26 **Abstract**

27 Bacterioplankton communities have a pivotal role in the global carbon cycle. Still the  
28 interaction between microbial community and dissolved organic matter (DOM) in freshwater  
29 ecosystems remains poorly understood. Here, we report results from a 12-day mesocosm  
30 study performed in the epilimnion of a tropical lake, in which inorganic nutrients and  
31 allochthonous DOM were supplemented under full light and shading. Although the  
32 production of autochthonous DOM triggered by nutrient addition was the dominant driver of  
33 changes in bacterial community structure, temporal covariations between DOM optical  
34 proxies and bacterial community structure revealed a strong influence of community shifts on  
35 DOM fate. Community shifts were coupled to a successional stepwise alteration of the DOM  
36 pool, with different fractions being selectively consumed by specific taxa. Typical freshwater  
37 clades as *Limnohabitans* and *Sporichthyaceae* were associated with consumption of low  
38 molecular weight carbon, whereas Gammaproteobacteria and Flavobacteria utilized higher  
39 molecular weight carbon, indicating differences in DOM preference among clades.  
40 Importantly, *Verrucomicrobiaceae* were important in the turnover of freshly produced  
41 autochthonous DOM, ultimately affecting light availability and dissolved organic carbon  
42 concentrations. Our findings suggest that taxonomically defined bacterial assemblages play  
43 definite roles when influencing DOM fate, either by changing specific fractions of the DOM  
44 pool or by regulating light availability and DOC levels.

45

46 **Keywords:**

47 Community structure, bacterioplankton, CDOM, mesocosm, Verrucomicrobiaceae

48

## 49 **Introduction**

50

51 Bacteria are key components of aquatic ecosystems playing crucial roles in  
52 biogeochemical cycles and ecosystem functioning (Lindeman, 1942; Pernthaler, 2005). Due  
53 to their metabolic diversity, morphology, large biomass, and high turnover rates, bacteria  
54 respond quickly to changes in catchments and associated water, affecting carbon cycling and  
55 energy transfer to higher levels in aquatic food webs (Cotner and Biddanda, 2002; Sanders et  
56 al., 2015). Freshwater ecosystems are exposed to a variety of stressors related to  
57 anthropogenic activities like elevated nutrient inputs and increases in organic matter runoff  
58 (Carpenter et al., 2011). Associated with such impacts are changes in rates of aquatic primary  
59 production and respiration, and alterations in the overall flux of carbon and composition of  
60 dissolved organic matter (DOM) (Bocaniov et al., 2013; Brandão et al., 2018). Despite  
61 differences in molecular size and degradability (Hansen et al., 2016), both autochthonous and  
62 allochthonous DOM fuel bacterial metabolism, affecting the availability of inorganic  
63 nutrients and organic carbon ultimately determining if autotrophic or heterotrophic energy  
64 mobilization will prevail (Jansson et al., 2007; Berglund et al., 2007).

65 The autochthonous DOM mainly consists of simple molecules (carbohydrates,  
66 proteins and amino acids) of low molecular weight (LMW) and is typically more labile for  
67 microbial community (Farjalla et al., 2009; Fonte et al., 2013). On the other hand, the  
68 allochthonous DOM is more susceptible to photodegradation because it contains relatively  
69 large molecules with high numbers of aromatic compounds, which strongly absorb UV light  
70 (Amon and Benner, 1994; McKnight et al., 1994; Benner, 2002; Helms et al., 2008). In this  
71 context, the chromophoric fraction of DOM (CDOM) constitutes an important and very  
72 variable pool of carbon, consisting of a continuum from labile to recalcitrant constituents  
73 (Rochelle-Newall et al., 2004, Benner and Amon, 2015). Bacterioplankton can increase the

74 amount of CDOM by transforming non-colored autochthonous DOM (Nelson et al., 2004;  
75 Asmala et al., 2018). Previous studies show that BCS varies with DOM composition and  
76 suggest ecological coherence between BCS and DOM composition (Judd et al., 2006; Amaral  
77 et al., 2016; Sarmiento et al., 2016). While community adaption (*i.e.* composition shifts) has  
78 been found to precede bacterial degradation of specific carbon substrates (Cory and Kling,  
79 2018), the contribution of BCS shifts and key bacterial players in the production and  
80 degradation of CDOM is unclear (Zhang et al., 2018).

81 Spectrophotometric analysis of CDOM is an important tool in studies of composition  
82 and origin of organic matter (Helms et al., 2008; Massicotte et al., 2017). Metrics extracted  
83 from the CDOM absorbance spectrum provide information on aromaticity  
84 ( $SUVA_{254}$ ; Weishaar et al., 2003), changes in relation to photo- ( $S_{275-295}$ ) and biodegradation  
85 ( $S_{350-400}$ ) (Helms et al., 2008), and changes in the relative size of DOM molecules ( $a_{250}: a_{365}$ ;  
86 De Haan and De Boer, 1987). Brandão et al. (2018) similarly used DOM optical proxies to  
87 infer a range of quantitative and qualitative changes observed during a factorial mesocosm  
88 experiment employing additions of allochthonous DOM and inorganic nutrients. Their results  
89 indicated that additions of allochthonous DOM affected CDOM absorption in the PAR range,  
90 with high influence of photodegradation. In contrast, more labile autochthonous DOM was  
91 degraded by bacteria, as suggested by Berggren et al. (2009).

92 Here, we applied a high-resolution taxonomic community analysis to characterize  
93 changes in the bacterioplankton and link this to the dynamics of the DOM pool documented  
94 by Brandão et al. (2018). By relating our findings to the DOM optical proxies described  
95 above, and results from the same mesocosm experiment (Tonetta et al., 2018; Brighenti et al.,  
96 2018), we aimed to provide insights on the interaction between DOM and BCS. By tracking  
97 down taxonomic signatures associated with specific changes in DOM, we expect a high  
98 degree of resource partitioning among bacterioplankton, as previously suggested for marine

99 waters (McCarren et al., 2010; Sarmiento et al., 2016). This presumption is endorsed by the  
100 great bacterioplankton diversity previously observed in the studied lake (Ávila et al., 2017).  
101 Additionally, the effect of direct and reduced sunlight was considered to investigate how  
102 photodegradation affects the association between BCS and DOM properties.

103

## 104 **Methods**

### 105 **Study area**

106 The data from this study originates from the mesocosm experiment described in detail  
107 by Brandão et al. (2018). In summary, the experiment was carried out in Lake Carioca  
108 (19°45'26.0''S; 42°37'06.2''W) located in the Rio Doce State Park, a remnant protected area  
109 of the Atlantic Forest (Minas Gerais, Brazil). This conservation unity is of great importance  
110 for global maintenance of biological diversity (<http://www.ramsar.org>). Lake Carioca is a  
111 small (perimeter: 1,718 m, area: 0.14 km<sup>2</sup>, volume: 671 x 10<sup>3</sup> m<sup>3</sup>, maximum depth: 11.8 m,  
112 mean depth: 4.8 m; Bezerra-Neto et al., 2010), turbid, mesotrophic and monomictic lake. The  
113 experiment was carried out in January, when Lake Carioca waters are found to be stratified  
114 (from September to April), increasing the lake euphotic zone depth and water transparency  
115 (Barbosa et al., 2012). Further characteristics of Lake Carioca can be found elsewhere  
116 (Brighenti et al., 2015; Reis et al., 2016).

117

### 118 **Mesocosm setup and water physico-chemical characterization**

119 The experiment was planned to mimic seasonal changes in inputs of allochthonous  
120 DOM and nutrients associated with variability in rain, water level and litter fall. It was  
121 carried out during summer 2015 (20<sup>th</sup> January to 1<sup>th</sup> February). Mesocosms (1.5 m height, 1.3  
122 m diameter and volume 2 m<sup>3</sup>) were installed in the upper mixed zone of the lake. The  
123 experiment applied a 2<sup>3</sup> factorial design with different combinations of inorganic nutrients

124 and allochthonous DOM additions and shading in two replicates each, totalizing 16  
125 mesocosms (Fig. S2). Each mesocosm was named according to the allochthonous DOM (C),  
126 inorganic nutrient (N), and light (L) in that particular order (*e.g.*, additions of allochthonous  
127 DOM and nutrient under shading: C<sup>+</sup>N<sup>+</sup>L<sup>-</sup>). Inorganic nutrient additions consisted of initial  
128 inoculation with nitrate (6.1 g of NaNO<sub>3</sub>), ammonium (0.42 g of NH<sub>4</sub>Cl) and phosphate (1.15  
129 g of K<sub>2</sub>HPO<sub>4</sub>) diluted in 40 ml of distilled water, resulting in initial concentrations of  
130 2,575 μg NO<sub>3</sub><sup>-</sup> L<sup>-1</sup>, 71 μg NH<sub>4</sub><sup>+</sup> L<sup>-1</sup> and 160 μg PO<sub>4</sub><sup>-3</sup> L<sup>-1</sup> at the amended bags. The  
131 allochthonous DOM consisted of fallen leaves, plant detritus and soil particles collected from  
132 forest floor bordering Lake Carioca. The litter material was dark-incubated for seven days at  
133 room temperature (32°C) in buckets filled with 60 L of distilled water without nutrient  
134 supplementation. Following, the admixture was filtered on a 62 μm mesh and 7.5 L of the  
135 filtrate were added in C<sup>+</sup> treatments, resulting in an initial concentration of 8.6 mg DOC L<sup>-1</sup>.  
136 To study the influence of the light availability in the mesocosms a shade net was placed  
137 reducing 50% of light irradiance. The efficacy of light attenuation was confirmed using a  
138 radiometer BIC (Biospherical Instruments, United States of America). The DOM proxies  
139 assessed were absorbance at 350 nm (*a*<sub>350</sub>), spectral slopes between 275-295 nm (*S*<sub>275-295</sub>) and  
140 350-400 nm (*S*<sub>350-400</sub>), DOC and its normalized absorbance at 254 nm (SUVA) and diffuse  
141 PAR attenuation coefficient (*K*<sub>dPAR</sub>). *a*<sub>350</sub> is a quantitative proxy of photo-absorbing DOM  
142 (De Haan and De Boer, 1987), *S*<sub>275-295</sub> and *S*<sub>350-400</sub> are qualitative indicators of photo- and  
143 biodegradable CDOM, respectively, and values are inversely proportional to CDOM  
144 molecular weight (Helms et al., 2008). SUVA indicates DOM aromaticity (Weishaar et al.,  
145 2003) and *K*<sub>dPAR</sub> is inversely proportional to the availability of light in the PAR range (Kirk  
146 1994), being both quantitative and qualitative proxies. All measurements and calculations  
147 were made as described by Brandão et al. (2018), except for *K*<sub>dPAR</sub> (Brandão et al., 2016).

148 Detailed information on the experimental design and measurements are described by  
149 Brighenti et al. (2018) and Tonetta et al. (2018).

150

### 151 **Sample collection**

152 Water samples (250 ml) from all 16 mesocosms were taken on days 1, 2, 3, 6, 9 and  
153 12, whereas on day 0 only the control (C<sup>-</sup>) and allochthonous DOM added (C<sup>+</sup>) mesocosms  
154 were sampled, as nutrient was added aseptically. Thus, we considered that initial differences  
155 in microbial communities were limited to microbes inoculated via allochthonous DOM  
156 addition. Samples were immediately transported to the laboratory, filtered (0.22 µm,  
157 Millipore, Billerica, MA, USA) and stored at -20°C until DNA extraction.

### 158 **DNA extraction, library construction, sequencing and qPCR**

159 Total DNA was extracted using the E.Z.N.A. ® Soil DNA Kit (OmegaBio-Tek) as  
160 recommended by the manufacturer and quantified with the Qubit fluorometer (Invitrogen-  
161 Life Technologies, USA). Following DNA isolation, paired-end libraries were constructed to  
162 assess the bacterial community composition using the primers S-D-Bact-0341-b-S-17/S-D-  
163 Bact-0785-a-A-21 (Klindworth et al., 2013), with Illumina adapters added, which target the  
164 V3-V4 regions of the 16S rRNA gene. The paired-end sequencing of the libraries was  
165 performed in an Illumina MiSeq platform (San Diego, CA, USA).

166 In order to assess the bacterial abundance, the 16S rRNA gene was estimated using  
167 the primer set 338F (5'TACGGGAGGCAGCAG3') (Lane et al., 1991) and 518R  
168 (5'ATTACCGCGGCTGCTGG3') (Muyzer et al., 1993), and the ABI 7900HT Fast Real-  
169 Time PCR System. (Applied Biosystems, Foster City, CA). Reaction conditions were as  
170 described by Reis et al. (2013).

171

172 **Bioinformatics**

173           After sequencing, raw reads were merged and processed using MOTHUR v.1.34.4  
174 (Schloss et al., 2009), including quality filtering (length < 400 and >430, without ambiguities  
175 and homopolymers > 8), chimera check and singleton exclusion using UCHIME (Edgar et  
176 al., 2011). The remaining reads were aligned and classified against the SILVA v.123 database  
177 (Quast et al., 2013) and clustered into operational taxonomic units (OTUs) using 3% as  
178 dissimilarity cutoff. Reads not classified into the Bacteria domain were removed (3 reads,  
179 representing <math>10^{-5}</math> of total).

180

181 **Data analysis**

182           All statistical analyses were performed in R (<https://www.r-project.org> - R Core Team  
183 2018) and the main steps performed are summarized in Figure S3. For alpha and beta  
184 diversity (PCoA) analyses reads assigned as Cyanobacteria and chloroplasts were removed  
185 from the dataset. Alpha diversity metrics (OTU richness and Simpson Evenness index) were  
186 determined after random normalization of reads counts at 1,629 reads depth. Changes in 16S  
187 abundance measures, alpha and beta diversity (described below), and DOM proxies were  
188 assessed using multiple linear regression analysis considering time, allochthonous DOM and  
189 nutrient additions and shade as explanatory variables, contemplating also first-order  
190 interactions. In order to evaluate regular time intervals and adjust community data to the  
191 same sampling frequency of DOM-related data, only samples from days 0, 3, 6, 9 and 12  
192 were considered. The percentages of Cyanobacteria and chloroplasts, which are derived from  
193 eukaryotic phototrophs, were calculated using the sum of the relative frequency of all reads  
194 classified as members of these groups, the remaining reads were assumed to represent  
195 bacterioplankton.



196 For Principal Coordinate Analysis (PCoA), beta diversity was calculated using all  
197 samples with more than 2,000 reads (3 out of 99 samples were removed: C<sup>-</sup>N<sup>+</sup>L<sup>+</sup> day 12,  
198 C<sup>+</sup>N<sup>-</sup>L<sup>+</sup> day 3 and C<sup>+</sup>N<sup>+</sup>L<sup>-</sup> day 9). After pruning these samples, a mean sample size of 57,562  
199 reads was observed. The normalization of reads per sample was based on cumulative sum  
200 scaling, as implemented by metagenomeSeq (Paulson et al., 2013), which conserves the  
201 relative proportion of species. Normalized OTU counts were further squared-root  
202 transformed and dissimilarity was calculated using weighted UniFrac distances (Lozupone et  
203 al., 2005) using the R-package phyloseq (McMurdie and Holmes, 2013). The input tree used  
204 for UniFrac distance calculation was generated in MOTHUR with the clearcut program  
205 (Evans et al., 2006), using the most abundant representative sequence of each OTU. The  
206 sample and OTU scores of the first three principal coordinates were subsequently extracted.  
207 The same procedure used to model the environmental variables was used to evaluate the  
208 relationship between the sample scores (response variable) and time, allochthonous DOM and  
209 nutrient additions and shade (explanatory variables).

210 To evaluate the synchronism in changes of DOM and BCS, a causality diagram was  
211 created to compare the outcomes from switching DOM proxies and principal coordinates  
212 extracted from the PCoA as factor and determinant on each other. Hence, it was tested  
213 whether temporal shifts in one type of variable ( $\Delta\text{PCoA}$  or  $\Delta\text{DOM}$ ) were correlated with  
214 preceding ( $\text{PCoA}^{\text{initial}}$  or  $\text{DOM}^{\text{initial}}$ ) or subsequent ( $\text{PCoA}^{\text{final}}$  or  $\text{DOM}^{\text{final}}$ ) levels of the other  
215 type of variable. Correlations likely indicate synchrony and were used to reveal positive and  
216 negative stimuli between community gradients (PCoA axis) and DOM proxies. This was  
217 done by comparing all possible combinations of linear regressions tested between DOM  
218 proxies and scores of the three main PCoA's axes: changes within a three-day interval in one  
219 hand ( $\Delta\text{PCoA}^{0-3}$  and  $\Delta\text{DOM}^{0-3}$  - response variable) versus either levels of the explanatory  
220 variable immediately before ( $\text{PCoA}^0$  and  $\text{DOM}^0$ ), or after ( $\text{PCoA}^3$  and  $\text{DOM}^3$ ) the three-day

221 shift. Resultant significant linear regressions ( $p$ -value  $< 0.05$ ) exhibiting a coefficient of  
222 determination ( $R^2$ )  $> 0.2$  were further considered and summarized in the causality diagram.  
223 The time interval of three days was chosen based on results from an experiment performed  
224 during field campaign in which carbon lability was inferred from daily changes of  $p\text{CO}_2$   
225 levels in dark incubations at  $30^\circ\text{C}$ , similar to lake conditions. Within three days, all treatments  
226 except one ( $\text{C}^+\text{N}^+\text{L}^+$ ) had achieved maximum carbon remineralization, as  $p\text{CO}_2$  reached the  
227 highest values, decreasing afterwards (Fig. S4).

228 To identify the taxonomic groups associated with each PCoA axis, the dispersion of  
229 OTU scores was inspected at different taxonomic levels. Plots were made to show the most  
230 abundant taxa considering pre-determined cut-offs of OTU richness per hierarchy, as follow  
231 30, 25, 15 and 10 for phylum, class, family and genus, respectively. An additional selection  
232 for a class final plot considered the five highest and lowest mean scores presented by taxon  
233 for all PCoA axes, whereas for family and genus, the eight highest and lowest mean scores  
234 were selected for each axis. Plots were drawn using the `geom_violin` function in the `ggplot2`  
235 package (Wickham et al., 2016), a feasible way to incorporate the density (i.e., indicating  
236 number of OTUs) along axis scores, thus illustrating the PCoA axis scores interval which a  
237 given taxon displays increased OTU richness. Finally, in order to reduce the number of taxa  
238 displayed and depict the distribution of OTUs over the three PCoA axis in an easily  
239 comparable fashion, trilinear plots were built using the function `ggtern` (Hamilton and Ferry,  
240 2018). The taxa chosen for the plots represented the 12 (phylum and class) and 16 (family  
241 and genus) bacterial groups, which better illustrated the different occurrence patterns  
242 observed for each hierarchic level. Each plot shows all OTUs of a given taxonomy in relation  
243 to their normalized PCoA species scores:  $\text{PCoA1} + \text{PCoA2} + \text{PCoA3} = 1$  (100%). Colored  
244 areas represent the OTUs distribution density according to a Gaussian kernel estimator  
245 implemented in the `stat_density_tern` function in `ggtern`.

246 All sequences were submitted to the Sequence Read Archive  
247 (<http://www.ncbi.nlm.nih.gov/sra/>) under the BioProject ID PRJNA515842.

248

## 249 **Results**

250

### 251 **Changes in microbial characteristics and DOM-related proxies**

252 The effect of shading and additions of nutrient and allochthonous DOM on microbial  
253 aspects (*i.e.* 16S abundance, richness, evenness and relative abundance of heterotrophs and  
254 phototrophs) of the mesocosms are shown in Figure 1 and Table 1. We did not observe  
255 influence of light in microbial measurements ( $p>0.05$ ). C<sup>+</sup> and N<sup>+</sup> mesocosms presented  
256 similar increases in 16S mean abundance (331.0 and 291.1%, respectively). Community  
257 richness was higher in C<sup>+</sup> mesocosms (25.5%), particularly at the beginning of the experiment  
258 due to the inoculation of allochthonous DOM-associated microbes. However, a reduction  
259 over time (-1.9% per day) was observed, thereby neutralizing the initial enrichment.  
260 Bacterioplankton relative abundance and community evenness diminished in N<sup>+</sup> treatments  
261 over time (-2.9% and -3.1% per day, respectively), with strongest effects on bacterioplankton  
262 relative abundance. The relative abundance of Cyanobacteria was reduced by allochthonous  
263 DOM addition (-5.8% per day) and increased by nutrient addition (5.3% per day). The  
264 relative abundance of chloroplasts was also reduced in treatment C<sup>+</sup> (-86.0%) and increased  
265 in N<sup>+</sup> (65.3%) considering total changes, however both additions caused daily increases of  
266 18.0 and 8.4%, respectively.

267 Differently from microbial parameters, changes in DOM optical properties to  
268 manipulations were overall stronger and significant for all treatments, including shading (Fig.  
269 2 and Table 2). Allochthonous DOM addition strongly decreased the S<sub>275-295</sub> (-13.3%) and  
270 S<sub>350-400</sub> (-6.5%) proxies and increased the DOC levels (8.7%), SUVA (17.2%) and a<sub>350</sub>

271 (56.5%) proxies. Nutrient addition increased  $a_{350}$  (9.1%) and decreased  $S_{275-295}$  (-2.2%),  
272 meanwhile shading contributed for a reduction of  $S_{275-295}$  (-0.3% per day),  $S_{350-400}$  (-1.1%)  
273 and increase in  $a_{350}$  (9.1% in  $N^-$  treatments, only).

274

## 275 **Bacterioplankton community structure**

276 Changes in BCS, assessed through a PCoA, showed that nutrient and allochthonous  
277 DOM additions affected community structure differently, while the effect of shading was  
278 inconclusive (Fig. 3). Allochthonous DOM addition promoted changes in BCS on day zero.  
279 This effect seems to have persisted in absence of nutrient supplementation, as the  
280 dissimilarity between  $N^+C^+$  and  $N^-C^-$  treatments was observed throughout the experiment. In  
281 contrast, pronounced changes observed in  $N^+$  treatments over time resulted in more similar  
282 communities, despite the allochthonous DOM addition. Between days 6 and 12, the  $N^+$   
283 communities experienced notable changes, segregating from  $N^-$  communities towards high  
284 PCoA1 and 2 scores.

285 The three main principal coordinates accounted for 57.5% of community variation  
286 (Fig. S5 and Table 3). PCoA1 was mainly influenced by the interaction between time and  
287 nutrient addition, increasing with a daily rate of 42.4%. A minor gain over time was also  
288 caused by allochthonous DOM addition (11.7% per day), as well as by time alone (10.5% per  
289 day). PCoA2 had a complex pattern of variance, mainly influenced by allochthonous DOM  
290 and nutrient additions. Initially, axis 2 was augmented in  $C^+$  treatments, however, as the  
291 scores suddenly decreased until day three, the overall effect of allochthonous DOM addition  
292 was weak and non-significant. Moreover, scores tended to diminish over time (-7.3% per  
293 day), except for  $N^+$  treatments, which increased at a daily rate of 9.2%. Differently from the  
294 other axes, in which a large score variation occurred during initial (PCoA2) or late (PCoA1  
295 and 2) periods, PCoA3 exhibited a pattern of variance defined by a scores' peak occurring on

296 day 3 and a second peak close to day 12. Although the effect of allochthonous DOM addition  
297 was not significant, the highest peak of PCoA3 scores was achieved in treatment C<sup>+</sup>N<sup>+</sup>,  
298 reflecting a further stimulation by allochthonous DOM addition.

299

### 300 **Linking DOM proxies and changes in BCS**

301 The assessment of synchrony in changes of the carbon pool and BCS suggested that  
302 the influence of BCS on DOM fate (Table 4,  $\Delta\text{PCoA}^{0-3} \sim \text{DOM}^3$  and  $\Delta\text{DOM}^{0-3} \sim \text{PCoA}^0$ ) was  
303 stronger than microbial adaptation in response to DOM (Table 5,  $\Delta\text{PCoA}^{0-3} \sim \text{DOM}^0$  and  
304  $\Delta\text{DOM}^{0-3} \sim \text{PCoA}^3$ ). Whereas quantitative DOM proxies as DOC and  $K_{d\text{PAR}}$  were both  
305 associated with PCoA1 and 3, qualitative proxies such as  $S_{350-400}$  were linked to PCoA2 and  
306 3, suggesting a disjuncture in the relationship between DOM and BCS (Tables 4 and 5). The  
307 optical proxies  $a_{350}$ , SUVA (both associated with PCoA3) and  $S_{275-295}$  (PCoA2) correlated to  
308 one principal coordinate each, indicating constricted associations with the bacterioplankton  
309 community. Therefore, PCoA1 was related to quantitative and PCoA2 was related to  
310 qualitative measures of DOM, while PCoA3 was related to both qualitative and quantitative  
311 proxies. Moreover, PCoA3 yielded stronger correlations with a larger number of proxies than  
312 the two other axes, likely representing a community fraction highly committed with DOM  
313 variation.

314 Figure 4 illustrates positive and negative associations between BCS and DOM-related  
315 proxies, as well as the effect of shading on these interactions. The spectral slopes were  
316 positively influenced by prior shifts in PCoA2. Decreases in  $S_{350-400}$ , which is a proxy related  
317 to biodegradable DOM, and increases in CDOM ( $a_{350}$ ) anticipated high PCoA3 scores. The  
318 influences of PCoA2 on  $S_{350-400}$  ( $R^2=0.46$  and  $p=0.003$ ) and of  $S_{350-400}$  ( $R^2=0.37$  and  $p=0.002$ )  
319 and  $a_{350}$  ( $R^2=0.27$  and  $p=0.01$ ) on PCoA3 were more predictable under shading (Figs. S6 and  
320 S7). PCoA3 was the major regulator of DOM-associated properties, affecting also DOM

321 aromaticity (SUVA) and quantity (DOC). The reason why the relationship between DOC  
322 levels and PCoA3 seemed dubious (Fig. 4), may be the pulse-like variation of PCoA3 scores  
323 over time (Fig. S5). Across the time series, PCoA3 peaks coincided with minimum DOC  
324 levels in most treatments (Fig. 2). Likewise, while high DOC levels anticipated gain of  
325 PCoA3 scores, increasing PCoA3 resulted in subsequent low DOC levels. Thus, the DOC  
326 increase observed after high PCoA3 scores was a consequence of the recovery of DOC levels  
327 posterior to high abundances of high-PCoA3 bacteria. Therefore, our results indicate that  
328 PCoA3 pulses were DOC-consuming events followed by low abundance of high-PCoA3  
329 bacteria, which lasted until newly synthesized DOC joined the DOM pool. Increases in  
330 PCoA1 scores contributed to restore DOC levels, especially without shading ( $R^2=0.39$  and  
331  $p=0.001$ , Fig. S8). Moreover, PCoA3 was also associated with the availability of light for  
332 photosynthesis ( $K_{dPAR}$ ), which has impacted PCoA1.

333

### 334 **Taxonomic assignment**

335        Figures 5 to 8 illustrate how the OTU richness of different bacterial groups changed in  
336 response to the main community drivers, as estimated by the first three PCoA axes. By  
337 evaluating the constraining effect of PCoA scores on taxa richness, we expected to obtain  
338 information on taxonomic adaptability in face of the observed changes in DOM pool. The  
339 dispersion of taxa richness over PCoA scores varied widely according to taxonomic level. As  
340 the PCoA scores varied widely over time (Fig. S9) and among treatments, the enrichment of  
341 taxa at specific ranges of PCoA scores indicated limited temporal and/or conditional  
342 occurrence (Figs. S10 to S13).

343        Overall, most phyla had OTU richness enlarged at low PCoA1 scores (Fig. 5). Within  
344 the four more abundant phyla, Actinobacteria and Verrucomicrobia were in line with this  
345 pattern, meanwhile among Proteobacteria and Bacteroidetes more OTUs with increased

346 PCoA1 were observed, suggesting enrichment at the final experimental days, especially in N<sup>+</sup>  
347 treatment (Fig. S10). At the class level, OTUs belonging to Alphaproteobacteria and  
348 Cytophagia achieved higher PCoA1 scores, whereas other classes like Spartobacteria,  
349 Acidimicrobiia and Clostridia were constrained to low scores (Fig. 6). Considering the  
350 observed association between PCoA1 and the proxies DOC and K<sub>dPAR</sub>, taxa exhibiting high  
351 PCoA1 scores as Cytophagia are likely associated with active DOC production under  
352 increased availability of light at the PAR range. This distribution pattern was observed for  
353 OTUs associated with the family Rhodobacteraceae (Fig. 6) and the genus *Tabrizicola* (Fig.  
354 8). Increases in DOC levels, water clarity (low K<sub>dPAR</sub>) (Fig. 4), density of plastid-associated  
355 producers, and pH were all positively associated with PCoA1 (Fig. S14). As some of these  
356 associations were more predictable under full light (Figs. S8 and S15), an increase in CO<sub>2</sub>  
357 availability due to photo-oxidation might have contributed to the enhancement of  
358 productivity (as discussed by Tonetta et al., 2018), consequently favoring high-PCoA1  
359 groups. Moreover, as the strongest declines in DOC levels occurred after rather than  
360 simultaneously to PCoA1 increases (Fig S16), the observed reduction in DOC levels was  
361 likely a consequence of DOM degradation by bacterial lineages exhibiting a pulse-like  
362 occurrence, like high-PCoA3 bacteria. Therefore, the associations between PCoA1 and the  
363 DOM pool resulted from the phytoplankton-associated production of autochthonous carbon  
364 rather than from a bacterioplankton-regulated process.

365 Axis 2 scores were low or intermediate for the dominant phyla. Actinobacteria  
366 (specially the Actinobacteria class) and Chloroflexi were remarkably enriched at low PCoA2  
367 scores, suggesting that these phyla exhibited preferences for late non-supplemented  
368 conditions (Figs. 5 and 6). In contrast, Firmicutes (except for Bacilli class) was markedly  
369 enriched at high PCoA2 scores found at C<sup>+</sup> treatment on the initial stage of the experiment,  
370 thereby implying an association with allochthonous DOM input. Such OTU distribution

371 pattern was exhibited by the families Veillonellaceae, Ruminococcaceae and  
372 Clostridiaceae\_1 (Firmicutes), likewise Sphingobacteriaceae (Bacteroidetes) (Fig. 7).  
373 Differently, three proteobacterial families (Oxalobacteraceae, Xanthomonadaceae and  
374 Pseudomonadaceae) distinctly presented reduction of OTUs as PCoA2 decreased. Regarding  
375 the PCoA2 association with qualitative CDOM proxies, these families were likely high  
376 molecular weight (HMW) carbon consumers supporting increases in  $S_{275-295}$  and  $S_{350-400}$ . In  
377 contrast, most families presenting low PCoA2 as Sporichthyaceae, LD12, FukuN57 and  
378 Saprospiraceae likely showed preferences for low molecular weight (LMW) carbon and  
379 contributed to the reduction of the spectral slopes.

380 Like axis 1, most phyla exhibited low PCoA3 scores (Fig. 5). Notably, slightly  
381 increased scores were detected for Verrucomicrobia and Planctomycetes. Taxa showing  
382 increased PCoA3 scores as the Verrucomicrobial families Verrucomicrobiaceae and P.  
383 palm\_C85 were likely involved in the PCoA3 peaks occurring on days 3 and 12 (Fig. 7). As  
384 assumed from the associations between PCoA3 and the DOM proxies, these taxa seem to  
385 play a role in CDOM consumption, reducing DOC levels and light attenuation in the PAR  
386 range. The regulation of DOC changes by bacteria linked with PCoA3 was stronger in  
387 nutrient supplemented treatments (Fig. S17). Verrucomicrobia *Prostheco bacter*, *Haloferula*  
388 and *Luteolibacter* were among genera that reached the highest PCoA3 values (Fig. 8), likely  
389 being typical representatives of this recycling lifestyle.

390

## 391 **Discussion**

392 Despite many previous studies have reported changes in BCS in response to DOM  
393 composition (Kritzberg et al., 2006; Judd et al., 2006; Gomez-Consarnau et al., 2012; Roiha  
394 et al., 2016; Smith et al., 2018), evidences for BCS influencing DOM characteristics are  
395 scarce (Guerrero-Feijóo et al., 2017; Goldberg et al., 2017; Wu et al., 2018). Our results



396 provide insights on links between observed changes in BCS and in the carbon pool, with  
397 community composition influencing and responding to specific DOM properties.  
398 Importantly, there was a strong influence of BCS on DOM processing and transformation,  
399 indicating that as some bacterial components use different substrates, they alter the DOM  
400 pool in specific ways. We also found that nutrients input was the main driver of  
401 bacterioplankton community and activity, either by enhancing microbial growth rates or  
402 through phytoplankton-DOM production, consistent with previous studies (Osterholz et al.,  
403 2016; Landa et al., 2016). Notably, our findings indicate that specific microbial members  
404 have potential impacts on changes in DOM pool molecular weight and suggest that a specific  
405 group, Verrucomicrobiaceae, plays a key role in CDOM turnover in these tropical waters.

#### 406 **Primary production as a driver of bacterial community changes**

407 The most pronounced change in BCS (PCoA1) was caused by nutrient addition,  
408 which furthermore enhanced air-water fluxes of CO<sub>2</sub> and O<sub>2</sub> (Tonetta et al., 2018), pelagic  
409 metabolic rates (Brighenti et al., 2018) and autochthonous DOC levels (Brandão et al., 2018).  
410 Our results also showed that PCoA1 was a proxy of a nutrient-induced impoverishment of  
411 bacterial diversity (Figs. 5 to 8). During the experiment, the heterotrophic activity was likely  
412 constrained as soon as the initially available labile carbon was respired, which happened  
413 briefly under nutrient supplementation, as shown by the sudden decreases in pCO<sub>2</sub> after the  
414 second day (Tonetta et al., 2018). In turn, simultaneous increases in PCoA1 scores, DOC  
415 levels, frequencies of Cyanobacteria and chloroplasts, together with decreases in  
416 bacterioplankton frequency and evenness were observed after day three in N<sup>+</sup> treatments,  
417 indicating that a “heterotrophic collapse” had occurred. In this sense, most taxa exhibiting  
418 low PCoA1 scores (Figs. 5 to 8) were likely outcompeted by phytoplankton and  
419 phytoplankton-associated bacteria. In addition to the effects of DOM and nutrient additions  
420 on BCS, pelagic community metabolism, including background bacterial respiration, were

421 also greatly affected (Brighenti et al., 2018). This supports previous findings that the growth  
422 rate of planktonic microorganisms is strongly depended on the availability of nutrients and  
423 labile DOM, favoring fewer and faster growing bacterial species rather than more diverse  
424 community under slower growth conditions (Sterner and Elser, 2002; Godwin and Cotner,  
425 2014).

426 Our results indicate that the class-level OTU classification discriminates  
427 phytoplankton-associated and/or fast-growing bacteria from groups with either limited  
428 capacity to directly compete with phytoplankton, or incapable of thriving under high  
429 productivity (Fig. 6). The latter represent the lake epilimnetic background community,  
430 particularly enriched by Actinobacteria and Verrucomicrobia, which are abundant phyla in  
431 Lake Carioca (Ávila et al., 2017). Moreover, a decrease in community evenness over time  
432 was observed specially for N<sup>+</sup> treatments, indicating that a few lineages colonized during  
433 periods of high primary production (*e.g.* classes Alphaproteobacteria and Cytophagia).  
434 Members of Alphaproteobacteria, especially the Rhodobacteraceae family, and Cytophagia  
435 have been consistently associated with phytoplankton-derived DOM (Eckert et al., 2012;  
436 Sarmento et al., 2016; Bunse et al., 2016). Within these groups, genera associated with high-  
437 PCoA1 scores, like *Tabrizicola*, have been found to be closely associated with phytoplankton  
438 in a symbiotic lifestyle (Cui et al., 2017), supporting a tight relation between high-PCoA1  
439 faster-growing lineages and primary producers. Lineages reaching high-PCoA1 scores were  
440 likely supported by a carbon substrate that might not transform the DOM pool (Lucas et al.,  
441 2016). Accordingly, bacteria associated with PCoA1 seems to involve fast-growing bacteria  
442 capable of rapidly incorporating freshly produced phytoplankton exudates (Fouilland et al.,  
443 2014). Indeed, preference for high concentrations of phytoplankton-derived DOM is  
444 suggested by the positive link between PCoA1 and DOC levels (Fig. S8). Sarmento et al.  
445 (2016) have shown that members of Bacteroidetes, which in our study exhibited high PCoA1

446 scores (classes Cytophagia and Flavobacteria), are more active with increasing  
447 phytoplankton-DOM concentration.

#### 448 **Changes in DOM quality and allochthonous DOM influence**

449 Shifts in BCS observed by the second principal component axis, PCoA2, were closely  
450 related to indices of DOM quality. Such shifts were initially influenced by allochthonous  
451 DOM addition, which induced notably high PCoA2 scores at day zero. However, nutrient  
452 addition also imposed a late increase in PCoA2 scores, suggesting that the influence of BCS  
453 on the qualitative DOM proxies  $S_{350-400}$  and  $S_{275-295}$  represent bacterial transformation of  
454 phytoplankton-produced and terrigenous carbon. These proxies are useful for tracking  
455 different pools of allochthonous and autochthonous DOM (Brandão et al., 2016). As  $S_{350-400}$   
456 and  $S_{275-295}$  both record changes in carbon molecular size (Helms et al., 2008), the enrichment  
457 of phyla exhibiting low PCoA2 scores, like Actinobacteria and Chloroflexi, likely contributed  
458 to the augment of DOM molecular weight. In contrast, reduction of DOM molecular weight  
459 resulted from the increased abundance of Saccharibacteria and Parcubacteria, which  
460 presented high-PCoA2. Importantly, full light seems to have hindered the effect of these BCS  
461 shifts on biodegradable DOM (Fig. S6), by blurring the association between changes in  
462 PCoA2-associated bacteria (especially LMW carbon consumers, as Sporichthyaceae,  
463 Saprospiraceae and FukuN57) and DOM quality. Oppositely, shading stimulated the bacterial  
464 groups competing for substrate with the photo-transformation processes, thereby stabilizing  
465 the influence of these taxa on DOM quality. Alternatively, an enhanced production of LMW  
466 autochthonous DOM was likely favored by reduced photoinhibition of phytoplankton in  
467 shaded treatments (Brighenti et al., 2018).

468 An alternative ecological interpretation of BCS shifts (here PCoA2), concerns the  
469 early stage of the experiment, when communities in  $C^+$  treatments showed remarkable  
470 changes (Fig. S9). The inoculation of bacteria-containing allochthonous litter strongly

471 affected BCS in C<sup>+</sup> treatments until day three, when all treatments exhibited very similar  
472 PCoA2 scores. Allochthonous bacteria were represented mainly by fermentative taxa  
473 belonging to Firmicutes (*e.g.* Ruminococaceae and Veillonellaceae, Fig. 7) and other  
474 lineages direct or indirectly associated with plant-polysaccharide degradation, as  
475 Saccharibacteria and *Mucilaginibacter* (Figs. 5 and 8, respectively) (Pankratov et al., 2007;  
476 Starr et al., 2018). Similarly to PCoA2 scores, OTU richness was immediately increased by  
477 allochthonous DOM supplementation (Fig. 1) and then diminished, suggesting that PCoA2  
478 also represented a strong selective pressure on allochthonous lineages in the lake. Therefore,  
479 genera highly abundant on C<sup>+</sup> treatments on day zero, like *Sporomusa*, had OTUs condensed  
480 at the higher limit of PCoA2 and were briefly cleared away, meanwhile *Burkholderia* has  
481 thrived later, exhibiting lower values of PCoA2, suggesting a short but higher persistency  
482 (Fig. 8). The rapid fading of inoculum-associated bacteria might have occurred due to high  
483 oxygen levels, which has probably constrained the occurrence of obligate anaerobes and  
484 microaerophiles within Clostridia and Negativicutes (Fig. 6) (Wiegel et al., 2006,  
485 Marchandin et al., 2010). In contrast, lineages as *Burkholderia*, which were also initially  
486 favoured by allochthonous DOM addition but resisted longer, were possibly benefited by its  
487 ability to tolerate oxidative stress conditions and to thrive in association with photodegraded  
488 organic matter (Paul et al., 2012). In comparison, the family level was more suitable than  
489 genus for detecting gradual and homogeneous changes throughout PCoA2 scores, thus  
490 allowing the recognition of taxa consistently contributing to the observed changes in DOM  
491 quality. As an example, increased richness of Sporichthyaceae and FukuN57 occurred  
492 downwards PCoA2 scores (Fig. 7). These taxa, together with the genera *Limnohabitans* and  
493 *Candidatus Aquirestis*, which also exhibited low PCoA2 (Fig. 8), are considered consumers  
494 of LMW carbon (Jones et al., 2009; Šimek et al., 2010; Eckert et al., 2012). In contrast,  
495 usually assumed as copiotrophic microbes (Nelson and Carlson, 2012; Landa et al., 2013),

496 gammaproteobacteria (families Xanthomonadaceae and Pseudomonadaceae) and  
497 Flavobacteriaceae presented enrichment at increasing PCoA2 scores, suggesting preference  
498 for HMW DOM as also previously suggested by Amaral et al. (2016) and Orsi et al. (2016).  
499 Importantly, Zhang et al. (2015) has shown that in oceanic waters, these groups are involved  
500 in the degradation of HMW exopolysaccharides potentially resulting in production of humic-  
501 like recalcitrant DOC, especially in replete N and P conditions. This could explain the  
502 association between high PCoA2 scores and increases in SUVA observed under nutrient  
503 supplementation (between days 0-3 and 9-12, Fig. 2), suggesting a participation of high-  
504 PCoA2 lineages in DOM aromatization. Therefore, as shifts in BCS as described above  
505 occur, they seem to affect and shape the DOM pool by depleting substrates of distinct  
506 molecular weight, thus contributing to changes in spectral slopes and overall DOM quality.

### 507 **CDOM recycling**

508 The third principal component axis (PCoA3) was a component of the bacterioplankton  
509 community highly committed to the observed changes in DOM pool (Fig. 4). Increases in  
510 PCoA3 scores resulted in lower DOC levels, which were subsequently recovered after the  
511 PCoA3 pulse (Table 4). The regulation of DOC changes by bacteria linked with PCoA3 were  
512 more robust in nutrient supplemented treatments (Fig. S17), suggesting that either PCoA3-  
513 associated bacteria recycle DOC under replete nutrient conditions, or present increased  
514 specificity for substrates produced in N<sup>+</sup> treatments. Additionally, as larger changes in DOC  
515 levels were more precisely predicted by PCoA3 under nutrient addition than in control,  
516 bacteria associated with PCoA3 should incorporate or respire autochthonous DOC efficiently.  
517 Also, as PCoA3 and 16S abundance simultaneously peaked on day 3, lineages exhibiting  
518 high PCoA3 scores should achieve high cell counts, which might explain the efficiency in  
519 regulating DOC levels and water transparency (Fig. 4). Our results also showed that  
520 reduction of S<sub>350-400</sub> and increase of a<sub>350</sub> induced high-PCoA3 bacteria under shading (Fig.

521 S7), suggesting that high-PCoA3 bacteria are active consumers of HMW, chromophoric  
522 DOC, which might be susceptible to photodegradation or have production hampered by  
523 photo-inhibition. Brandão et al. (2018) pointed out that during the experiment, autochthonous  
524 carbon production increased absorption at wavelengths above 350 nm, adding onto the  
525 contribution of freshly produced carbon on PCoA3. Intriguingly, our findings indicate that  
526 the Gammaproteobacteria-Flavobacteria (high-PCoA2) growth might have contributed to the  
527 PCoA3 pulses by producing HMW aromatic DOC, as high PCoA2 scores preceded pulses in  
528 PCoA3 (Fig. S9).

529         Our results showed that members of the Verrucomicrobiaceae family were enriched at  
530 high PCoA3 scores, notably OTUs associated with the genera *Prostheco bacter*, *Haloferula*,  
531 *Brevifollis* and *Luteolibacter* (Fig. 8). Although information concerning the roles of most  
532 verrucomicrobial groups in freshwater is still scarce, these genera have been found in  
533 different aquatic environments and their adaptive success rely on a broad repertoire of  
534 carbon-degrading enzymes (Martinez-Garcia et al., 2012; Zhang et al., 2014; Balmonte et al.,  
535 2016). Verrucomicrobiaceae have been previously associated with increases in  
536 phytoplankton-derived bioavailable DOM (Landa et al., 2013) and contribute to hydrolysis of  
537 complex HMW-polysaccharides (Cardman et al., 2014). Moreover, a metagenomic survey on  
538 freshwater Verrucomicrobia revealed an enrichment of Ton transporters genes (Cabello-  
539 Yeves et al., 2017), which code for proteins involved on complex HMW DOM cycling  
540 (McCarren et al., 2010). Therefore, our findings suggest that a few closely related lineages  
541 consume HMW DOM, most likely of autochthonous origin, indicating an ecologically  
542 coherent and exclusive role for Verrucomicrobiaceae in our experiment. This finding  
543 contributes to the current knowledge of bacterial taxa involved in the degradation of complex  
544 microbial-produced DOM, as data on microbial populations responsible for cycling  
545 recalcitrant DOM are still scarce (Zhang et al., 2018).

546 The DOM aspects linked to high-PCoA3 values concerned not only carbon quality  
547 ( $a_{350}$  and  $S_{350-400}$ ), but also decreased levels of DOC and PAR attenuation. This suggests that  
548 high-PCoA3 bacteria likely impacted water transparency, increasing light availability at  
549 wavelengths  $>400$  nm, resulting in a subsequent increased primary productivity and  
550 abundance of phototrophs. Likewise, high-PCoA3 bacteria seem to reduce the aromaticity of  
551 the DOM pool (SUVA decrease). Thus, high PCoA3-groups like Verrucomicrobiaceae,  
552 *Chthonomonas* (Armatimonadetes), *Parafilimonas* (Chitinophagaceae), *Oceanicoccus*  
553 (Gammaproteobacteria) and *Aquabacterium* (Betaproteobacteria) seem to be highly active in  
554 recycling DOM. Our results indicate that these bacteria are capable of sensing DOM changes  
555 (Fig. S7) and as response, controlling the CDOM fate (quantitatively and qualitatively) by  
556 efficiently consuming the accumulated aromatic HMW fraction of the DOM pool, impacting  
557 light availability and other community members, specially DOC producers.

558

## 559 **Conclusions**

560 Our results revealed consistent associations between distinct microbial groups and  
561 specific changes in the DOM pool over time, suggesting resource partitioning among  
562 bacterial groups, as previously reported for the microbial organic matter turnover in the sea  
563 (McCarren et al., 2010). We observed a dynamic control of community members on DOM  
564 fate, with specialized groups affecting distinct properties of DOM, likely contributing  
565 altogether to DOM recycling. The activity of each specialized group was time-dependent: as  
566 productivity increased and carbon molecular weight decreased, active consumers of HMW  
567 carbon and/or fast-growing strains were gradually replaced by other bacterial groups with  
568 affinity for LMW compounds. This exchange occurred concomitantly with a pulse of DOC-  
569 consuming, notably Verrucomicrobiaceae, showing preference for chromophoric carbon of  
570 autochthonous origin. Some lineages, as Flavobacteriaceae and Gammaproteobacteria might

571 have contributed to the production of such complex chromophoric DOM pool. Although the  
572 succession pattern described above also occurred in the control (Fig. S9), increasing DOM  
573 and nutrient resources enhanced the magnitude of the microbial shifts, likely due to an  
574 augmented availability of substrate leading to a higher abundance of the favored groups.  
575 Lineages tightly linked to autochthonous carbon production (PCoA1) reflected this trend  
576 quantitatively, changing proportionally to the density of primary producers, which imposed a  
577 high restraint on background communities. Moreover, the switch between Flavobacteria-  
578 Gammaproteobacteria and Sporichthyaceae-LD12 groups seems to regulate DOM quality,  
579 and distinguished bacterial groups based on molecular weight affinity.

580 Therefore, our findings claim attention for a verrucomicrobial family  
581 (Verrucomicrobiaceae) and other taxa as *Chthonomonas* and *Aquabacterium* as short-lived  
582 but yet important recyclers of DOM affecting water clarity and re-fueling primary  
583 production. These findings expand the basis for future investigations aiming to deep the  
584 comprehension of DOM cycling in tropical lakes, which might validate the efficiency of  
585 these microbial players as major lineages responsible for CDOM remineralization. Finally,  
586 our study confirms that different sources of DOM impact specific bacterial groups  
587 differently. More importantly, our findings suggest that taxonomically defined assemblages  
588 play definite roles when influencing DOM fate, either by changing specific fractions of the  
589 DOM pool or by regulating DOC levels.

590

## 591 **Acknowledgements**

592 This work was supported by the Fundação de Amparo à Pesquisa do Estado de Minas Gerais  
593 (FAPEMIG); Conselho Nacional de Desenvolvimento Científico e Tecnológico (CNPq); and  
594 Coordenação de Aperfeiçoamento de Pessoal de Nível Superior (CAPES) through the project  
595 Carbon Cycling in Lakes (COCLAKE – CAPES Proc. no 88881.030499/2013-01). We would



596 like to thank Gustavo Turci, Patrícia Ferreira and Ralph Thomé for field support. We also  
597 thank Diego Pujoni for his valuable suggestions and Anderson Carmo for the support during  
598 DNA sequencing at LBMM-ICB-UFMG.

599

## 600 **Figure legends**

601 **Figure 1:** Temporal variation of alpha diversity (OTU richness and evenness – Simpson  
602 1/D), 16S copy number, and percentages of bacterioplankton, cyanobacteria and chloroplast-  
603 associated reads. Values represent means  $\pm$  SE. Red and black colours depict treatments with  
604 and without allochthonous DOM addition, respectively. Triangle and circle symbols  
605 correspond to treatments with and without nutrient addition, respectively. Solid lines  
606 represent shaded treatments and dashed lines indicate full light.

607

608 **Figure 2:** Temporal variation of  $a_{350}$ ,  $S_{275-295}$ ,  $S_{350-400}$ , dissolved organic carbon (DOC),  
609 SUVA and  $K_{dPAR}$ . Values represent means  $\pm$  SE. Red and black colours depict treatments  
610 with and without allochthonous DOM addition, respectively. Triangle and circle symbols  
611 correspond to treatments with and without nutrient addition, respectively. Solid lines  
612 represent shaded treatments and dashed lines indicate full light.

613

614 **Figure 3:** Temporal variation of PCoA1, 2 and 3. Values represent means  $\pm$  SE. Red and  
615 black colours depict treatments with and without allochthonous DOM addition, respectively.  
616 Triangle and circle symbols correspond to treatments with and without nutrient addition,  
617 respectively. Solid lines represent shaded treatments and dashed lines indicate full light.

618

619 **Figure 4:** Diagram illustrating the synchronism between shifts in bacterioplankton  
620 community structure and DOM proxies. Detailed statistics are shown on Tables 4 and 5.

621 Quantitative, quantitative/qualitative and qualitative proxies are represented by ellipses,  
622 triangles and rectangles, respectively. Red and green lines represent negative and positive  
623 associations, respectively. Solid and dashed lines represent significant linearity between a  
624 three-day shift ( $\Delta\text{PCoA}^{0-3}$  and  $\Delta\text{DOM}^{0-3}$ ) and the associated explanatory variable  
625 immediately before ( $\text{PCoA}^0$  and  $\text{DOM}^0$ ), or after ( $\text{PCoA}^3$  and  $\text{DOM}^3$ ) the shift, respectively.  
626 Black and yellow stars represent increased fitness of the association under shading and full-  
627 light, respectively.

628

629 **Figure 5:** Ternary plot showing all OTUs of 12 different phyla chosen to represent distinct  
630 patterns of occurrence in relation to the three main PCoA axis. Each circle represents one  
631 OTU positioned according to the normalized contribution of the indicated PCoA axis (species  
632 score):  $\text{PCoA1} + \text{PCoA2} + \text{PCoA3} = 1$  (100%). Colored areas depict the density (Gaussian  
633 kernel estimator) of the OTUs distribution. The number between parenthesis indicates the  
634 total richness of OTUs for each phylum.

635

636 **Figure 6:** Ternary plot showing all OTUs of 12 different classes chosen to represent distinct  
637 patterns of occurrence in relation to the three main PCoA axis. Each circle represents one  
638 OTU positioned according to the normalized contribution of the indicated PCoA axis (species  
639 score):  $\text{PCoA1} + \text{PCoA2} + \text{PCoA3} = 1$  (100%). Colored areas depict the density (Gaussian  
640 kernel estimator) of the OTUs distribution. The number between parenthesis indicates the  
641 total richness of OTUs for each class.

642

643 **Figure 7:** Ternary plot showing all OTUs of 16 different families chosen to represent distinct  
644 patterns of occurrence in relation to the three main PCoA axis. Each circle represents one  
645 OTU positioned according to the normalized contribution of the indicated PCoA axis (species

646 score):  $PCoA1 + PCoA2 + PCoA3 = 1$  (100%). Colored areas depict the density (Gaussian  
647 kernel estimator) of the OTUs distribution. The number between parenthesis indicates the  
648 total richness of OTUs for each family.

649

650 **Figure 8:** Ternary plot showing all OTUs of 16 different genera chosen to represent distinct  
651 patterns of occurrence in relation to the three main PCoA axis. Each circle represents one  
652 OTU positioned according to the normalized contribution of the indicated PCoA axis (species  
653 score):  $PCoA1 + PCoA2 + PCoA3 = 1$  (100%). Colored areas depict the density (Gaussian  
654 kernel estimator) of the OTUs distribution. The number between parenthesis indicates the  
655 total richness of OTUs for each genus.

## 656 **References**

657 Amaral, V., Graeber, D., Calliari, D., Alonso, C., 2016. Strong linkages between DOM  
658 optical properties and main clades of aquatic bacteria. *Limnol. Oceanogr.* 61: 906–918.

659 Amon, R.M.W., Benner, R., 1994. Rapid cycling of high-molecular-weight dissolved organic  
660 matter in the ocean. *Nature.* 369: 549–552.

661 Asmala, E., Haraguchi, L., Carstensen, J., Jakobsen, H., Massicotte, P., 2018. Nutrient  
662 availability as major driver of phytoplankton- derived dissolved organic matter  
663 transformation in coastal environment. *Biogeochemistry.* 137: 93–104.

664 Ávila, M.P., Staehr, P.A., Barbosa, F.A.R., Chartone-Souza, E., Nascimento, A.M.A., 2017.  
665 Seasonality of freshwater bacterioplankton diversity in two tropical shallow lakes from the  
666 Brazilian Atlantic Forest. *FEMS Microbiol. Ecol.* 93: 10.1093/femsec/fiw218

667 Barbosa, L.G, Barbosa, F.A.R., Bicudo, C.E.M., 2012. Inter-annual chemical stratification in  
668 Brazilian natural lakes: meromixis and hypolimnetic memory. *Acta Limnologica Brasiliensia*.  
669 24: 127–139.

670 Balmonte, J.P., Arnosti, C., Underwood, S., Mckee, B.A., 2016. Riverine bacterial  
671 communities reveal environmental disturbance signatures within the Betaproteobacteria and  
672 Verrucomicrobia. *Front. Microbiol.* 7: 1441.

673 Benner, R. 2002. Chemical composition and reactivity. 59–90. *Biogeochemistry of marine*  
674 *dissolved organic matter*, Elsevier Science.

675 Benner, R., Amon, R.M.W., 2015. The size-reactivity continuum of major bioelements in the  
676 ocean. *Annu. Rev. Mar. Sci.* 7: 185–205.

677 Berggren, M., Laudon, H., Jansson, M., 2009. Aging of allochthonous organic carbon  
678 regulates bacterial production in unproductive boreal lakes, *Limnol. Oceanogr.* 54: 1333–  
679 1342.

680 Berglund, J., Müren, U., Båmstedt, U., Andersson, A., 2007. Efficiency of a phytoplankton-  
681 based and a bacteria-based food web in a pelagic marine system. *Limnol. Oceanogr.* 52: 121  
682 – 131.

683 Bezerra-Neto, J.F., Brighenti, L.S., Pinto-Coelho, R.M., 2010. A new morphometric study of  
684 Carioca Lake, Parque Estadual do Rio Doce (PERD), Minas Gerais State, Brazil. *Acta Sci*  
685 *Biol Sci.* 32: 49–54.

686 Bocaniov, S.A., Barton, D.R., Schiff, S.L., Smith, R.E.H., 2013. Impact of tributary DOM  
687 and nutrient inputs on the nearshore ecology of a large, oligotrophic lake (Georgian Bay,  
688 Lake Huron, Canada). *Aquat. Sci.* 75: 321–332.

689 Brandão, L.P.M., Staehr, P.A., Bezerra-Neto, J.F., 2016. Seasonal changes in optical  
690 properties of two contrasting tropical freshwater systems. *J. Limnol.* 75: 18.

691 Brandão, L.P.M., Brighenti, L.S., Staehr, P.A., Asmala, E., Massicotte, P., Tonetta, D.,  
692 Barbosa, F.A.R., Pujoni, D., et al., 2018. Distinctive effects of allochthonous and  
693 autochthonous organic matter on CDOM spectra in a tropical lake. *Biogeosciences.* 15:  
694 2931–2943.

695 Brighenti, L.S., Staehr, P.A., Gagliardi, L.M., Brandão, L.P.M., Elias, E.C., de Mello,  
696 N.A.S.T., Barbosa, F.A.R., Bezerra-Neto, J.F., 2015. Seasonal changes in metabolic rates of  
697 two tropical lakes in the Atlantic Forest of Brazil. *Ecosystems.* 18: 589–604.

698 Brighenti, L.S., Staehr, P.A., Brandão, L.P.M., Barbosa, F.A.R., Bezerra-Neto, J.F., 2018.  
699 Importance of nutrients, organic matter and light availability on epilimnetic metabolic rates in  
700 a mesotrophic tropical lake. *Freshwater Biol.* 63: 1143–1160.

701 Bunse, C., Bertos-Fortis, M., Sassenhagen, I., Sildever, S., Sjöqvist, C., Godhe, A., Gross, S.,  
702 Kremp, A., et al., 2016. Spatio-temporal interdependence of bacteria and phytoplankton  
703 during a baltic sea spring bloom. *Front. Microbiol.* 7: 517. doi: 10.3389/fmicb.2016.00517

704 Cabello-Yeves, P.J., Ghai, R., Mehrshad, M., Picazo, A., Camacho, A., Rodriguez-Valera, F.,  
705 2017. Reconstruction of diverse verrucomicrobial genomes from metagenome datasets of  
706 freshwater reservoirs. *Front. Microbiol.* 8: 2131. doi: 10.3389/fmicb.2017.02131

707 Cardman, Z., Arnosti, C., Durbin, A., Ziervogel, K., Cox, C., Steen, A.D., Teske, A., 2014.  
708 Verrucomicrobia are candidates for polysaccharide-degrading bacterioplankton in an Arctic  
709 fjord of Svalbard. *Appl. Environ. Microbiol.* 80: 3749–3756.

710 Carpenter, S.R., Stanley, E.H., Zanden, M.J.V., 2011. State of the world's freshwater  
711 ecosystems: physical, chemical, and biological changes. *Annu. Rev. Environ. Resour.* 36: 75–  
712 99.

713 Cory, R.M., Kling, G.W., 2018. Interactions between sunlight and microorganisms influence  
714 dissolved organic matter degradation along the aquatic continuum. *Limnol. Oceanogr.*  
715 *Letters.* 3: 102–116.

716 Cotner, J.B., Biddanda, B.A., 2002. Small players, large role: microbial influence on  
717 biogeochemical processes in pelagic aquatic ecosystems. *Ecosystems.* 5: 105–121.

718 Cui, Y., Jin, L., Ko, S.R., Chun, S.J., Oh, H.S., Lee, C.S., Srivastava, A., Oh, H.M., et al.,  
719 2017. Periphyton effects on bacterial assemblages and harmful cyanobacterial blooms in a  
720 eutrophic freshwater lake: a mesocosm study. *Sci. Rep.* 7: 7827.

721 De Haan, H., De Boer, T., 1987. Applicability of light absorbance and fluorescence as  
722 measures of concentration and molecular size of dissolved organic carbon in humic Laken  
723 Tjeukemeer. *Water Res.* 21: 731–734.

724 Eckert, E.M., Salcher, M.M., Posch, T., Eugster, B., Pernthaler, J., 2012. Rapid successions  
725 affect microbial N-acetyl-glucosamine uptake patterns during a lacustrine spring  
726 phytoplankton bloom. *Environ. Microbiol.* 14: 794–806.

727 Edgar, R.C., Haas, B.J., Clemente, J.C., Quince, C., Knight, R., 2011. UCHIME improves  
728 sensitivity and speed of chimera detection. *Bioinformatics* 27: 2194–2200.

729 Evans, J., Sheneman, L., Foster J.A., 2006. Relaxed Neighbor-Joining: A Fast Distance-  
730 Based Phylogenetic Tree Construction Method. *J. Mol. Evol.* 62: 785-792.

731 Farjalla, V.F., Marinho, C.C., Faria, B.M., Amado, A.M., Esteves, F.D.A., Bozelli, R.L.,  
732 Giroldo, D., 2009. Synergy of fresh and accumulated organic matter to bacterial growth.  
733 *Microb. Ecol.* 57: 657–666.

734 Fonte, E.S., Amado, A.M., Meirelles-Pereira, F., Esteves, F.A., Rosado, A.S., Farjalla, V.F.,  
735 2013. The combination of different carbon sources enhances bacterial growth efficiency in  
736 aquatic ecosystems. *Microb. Ecol.* 6: 871–878.

737 Fouilland, E., Tolosa, I., Bonnet, D., Bouvier, C., Bouvier, T., Bouvy, M., Got, P., Le Floc'h,  
738 E., et al., 2014. Bacterial carbon dependence on freshly produced phytoplankton exudates  
739 under different nutrient availability and grazing pressure conditions in coastal marine waters.  
740 *FEMS Microbiol. Ecol.* 87: 757–769.

741 Godwin, C.M., Cotner, J.B., 2014. Carbon:phosphorus homeostasis of aquatic bacterial  
742 assemblages is mediated by shifts in assemblage composition. *Aquat. Microb. Ecol.* 73: 245–  
743 258.

744 Goldberg, S.J., Nelson, C.E., Viviani, D.A., Shulse, C.N., Church, M.J., 2017. Cascading  
745 influence of inorganic nitrogen sources on DOM production, composition, lability and  
746 microbial community structure in the open ocean. *Environ. Microbiol.* 19: 3450–3464.

747 Gomez-Consarnau, L., Lindh, M.V., Gasol, J.M., Pinhassi, J., 2012. Structuring of  
748 bacterioplankton communities by specific dissolved organic carbon compounds. *Environ.*  
749 *Microbiol.* 14: 2361–2378.

750 Guerrero-Feijóo, E., Nieto-Cid, M., Sintes, E., Dobal-Amador, V., Hernando-Morales, V.,  
751 Álvarez, M., Balagué, V., Varela, M.M., 2017. Optical properties of dissolved organic matter

752 relate to different depth-specific patterns of archaeal and bacterial community structure in the  
753 North Atlantic Ocean. *FEMS Microbiol. Ecol.* 93: 1–14.

754 Hamilton, N.E., Ferry, M., 2018. “ggtern: Ternary Diagrams Using ggplot2.” *Journal of*  
755 *Statistical Software, Code Snippets*, 87: 1–17.

756 Hansen, A.M., Kraus, T.E.C., Pellerin, B.A., Fleck, J.A., Downing, B.D., Bergamaschi, B.A.,  
757 2016. Optical properties of dissolved organic matter (DOM): Effects of biological and  
758 photolytic degradation. *Limnol. Oceanogr.* 61: 1015–1032.

759 Helms, J.R., Stubbins, A., Ritchie, J.D., Minor, E.C., Kieber, D.J., Mopper, K., 2008.  
760 Absorption spectral slopes and slope ratios as indicators of molecular weight, source, and  
761 photobleaching of chromophoric dissolved organic matter. *Limnol. Oceanogr.* 53: 955–969.

762 Jansson, M., Persson, L., De Roos, A.M., Jones, R.I., Tranvik, L.J., 2007. Terrestrial carbon  
763 and intraspecific size-variation shape lake ecosystems. *Trends in Ecology & Evolution.* 22:  
764 316–22.

765 Jones, S.E., Newton, R.J., McMahon, K.D., 2009. Evidence for structuring of bacterial  
766 community composition by organic carbon source in temperate lakes. *Environ. Microbiol.* 11:  
767 2463–72.

768 Judd, K.E., Crump, B.C., Kling, G.W., 2006. Variation in dissolved organic matter controls  
769 bacterial production and community composition. *Ecology.* 87: 2068–2079.

770 Kirk, J.T.O., 1994. *Light and photosynthesis in aquatic ecosystems.* Cambridge University  
771 Press.



772 Klindworth, A., Pruesse, E., Schweer, T., Peplies, J., Quast, C., Horn, M., Glöckner, F.O.,  
773 2013. Evaluation of general 16S ribosomal RNA gene PCR primers for classical and next-  
774 generation sequencing-based diversity studies. *Nucleic Acids Research*. 41(1): e1. doi:  
775 10.1093/nar/gks808

776 Kritzberg, E.S., Langenheder, S., Lindström, E.S., 2006. Influence of dissolved organic  
777 matter source on lake bacterioplankton structure and function - Implications for seasonal  
778 dynamics of community composition. *FEMS Microbiol. Ecol.* 56: 406–417.

779 Landa, M., Cottrell, M.T., Kirchman, D.L., Blain, S., Obernosterer, I., 2013. Changes in  
780 bacterial diversity in response to dissolved organic matter supply in a continuous culture  
781 experiment. *Aquat. Microb. Ecol.* 69: 157–168.

782 Landa, M., Blain, S., Christaki, U., Monchy, S., Obernosterer, I., 2016. Shifts in bacterial  
783 community composition associated with increased carbon cycling in a mosaic of  
784 phytoplankton blooms. *ISME J.* 10: 39–50.

785 Lane, D.J., 1991. 16S/23S rRNA sequencing (pp. 115–175). In E. Stackebrandt, & M.  
786 Goodfellow (Eds.), *Nucleic acid techniques in bacterial systematics*, New York, USA: John  
787 Wiley and Sons.

788 Lindeman, R.L., 1942. The trophic-dynamic aspect of ecology. *Ecology*. 23: 399–418.

789 Lozupone, C., Knight, R., 2005. UniFrac: a new phylogenetic method for comparing  
790 microbial communities. *App. Environ. Microbiol.* 71: 8228–8235.

791 Lucas, J., Koester, I., Wichels, A., Niggemann, J., Dittmar, T., Callies, U., Wiltshire, K.H.,  
792 Gerds, G., 2016. Short-term dynamics of North Sea bacterioplankton-dissolved organic  
793 matter coherence on molecular level. *Front. Microbiol.* 7: 1–14.

794 Marchandin, H., Teyssier, C., Campos, J., Jean-Pierre, H., Roger, F., Gay, B., Carlier, J.P.,  
795 Jumas-Bilak, E., 2010. *Negativicoccus succinicivorans* gen. nov., sp. nov., isolated from  
796 human clinical samples, emended description of the family Veillonellaceae and description of  
797 *Negativicutes* classis nov., *Selenomonadales* ord. nov. and *Acidaminococcaceae* fam. nov. in  
798 the bacterial phylum Firmicutes. *Int. J Syst. Evol. Microbiol.* 60: 1271–1279.

799 Martinez-Garcia, M., Brazel, D.M., Swan, B.K., Arnosti, C., Chain, P.S., Reitenga, K.G.,  
800 Xie, G., Poulton, N.J., et al., 2012. Capturing single cell genomes of active polysaccharide  
801 degraders: an unexpected contribution of Verrucomicrobia. *PLoS One.* 7: e35314.

802 Massicotte, P., Asmala, E., Stedmon, C., Markager, S., 2017. Global distribution of dissolved  
803 organic matter along the aquatic continuum: Across rivers, lakes and oceans. *Sci. Tot.*  
804 *Environ.* 609: 180–191.

805 McCarren, J., Becker, J.W., Repeta, D.J., Shi, Y., Young, C.R., Malmstrom, R.R., Chisholm,  
806 S.W., DeLong, E.F., 2010. Microbial community transcriptomes reveal microbes and  
807 metabolic pathways associated with dissolved organic matter turnover in the sea. *Proc. Natl.*  
808 *Acad. Sci.* 107: 16420–16427.

809 McKnight, D.M., Andrews, E.D., Spaulding, S.A., Aiken, G.R., 1994. Aquatic fulvic acids in  
810 algal-rich antarctic ponds. *Limnol. Oceanogr.* 39: 1972–1979.

811 McMurdie, P.J., Holmes, S., 2013. phyloseq: an R package for reproducible interactive  
812 analysis and graphics of microbiome census data. *PLoS ONE.* 8(4): e61217.

813 Muyzer, G., de Waal, E.C., Uitterlinden, G., 1993. Profiling of complex microbial  
814 populations by denaturing gradient gel electrophoresis analysis of polymerase chain reaction-  
815 amplified genes coding for 16S rRNA. *Appl. Environ. Microbiol.* 59: 695–700.

816 Nelson, C.E., Carlson, C.A., 2012. Tracking differential incorporation of dissolved organic  
817 carbon types among diverse lineages of Sargasso Sea bacterioplankton. *Environ. Microbiol.*  
818 14: 1500–1516.

819 Nelson, N.B., Carlson, C.A., Steinberg, D.K., 2004. Production of chromophoric dissolved  
820 organic matter by Sargasso Sea microbes. *Mar. Chem.* 89: 273–287.

821 Orsi, W.D., Smith, J.M., Liu, S., Liu, Z., Sakamoto, C.M., Wilken, S., Poirier, C., Richards,  
822 T.A., 2016. Diverse, uncultivated bacteria and archaea underlying the cycling of dissolved  
823 protein in the ocean. *ISME J.* 10: 2158–2173.

824 Osterholz, H., Singer, G., Wemheuer, B., Daniel, R., Simon, M., Niggemann, J., Dittmar, T.,  
825 2016. Deciphering associations between dissolved organic molecules and bacterial  
826 communities in a pelagic marine system. *ISME J.* 10: 1717–1730.

827 Pankratov, T.A., Tindall, B.J., Liesack, W., Dedysh, S.N., 2007. *Mucilaginibacter paludis*  
828 gen. nov., sp. nov. and *Mucilaginibacter gracilis* sp. nov., pectin-, xylan and laminarin-  
829 degrading members of the family Sphingobacteriaceae from acidic Sphagnum peat bog. *Int.*  
830 *J. Syst. Evol. Microbiol.* 57: 2349–2354.

831 Paul, A., Dziallas, C., Zwirnmann, E., Gjessing, E.T., Grossart, H.P., 2012. UV irradiation of  
832 natural organic matter (NOM): Impact on organic carbon and bacteria. *Aquat. Sci.* 74: 443–  
833 454.

834 Paulson, J.N., Stine, O.C., Bravo, H.C., Pop, M., 2013. Differential abundance analysis for  
835 microbial marker-gene surveys. *Nature Methods.* 10: 1200–1202.

836 Pernthaler, J., 2005. Predation on prokaryotes in the water column and its ecological  
837 implications. *Nat. Rev. Microbiol.* 3: 537–547.

838 Quast, C., Pruesse, E., Yilmaz, P., Gerken, J., Schweer, T., Yarza, P., Peplies, J., Glöckner,  
839 F.O., 2013. The SILVA ribosomal RNA Gene Database Project: improved data processing  
840 and web-based tools. *Nucleic Acids Research*. 41(Database issue): D590–D596. <https://doi.org/10.1093/nar/gks1219>  
841

842 Reis, M.P., Barbosa, F.A.R., Chartone-Souza, E., Nascimento, A.M.A., 2013. The  
843 prokaryotic community of a historically mining-impacted tropical stream sediment is as  
844 diverse as that from a pristine stream sediment. *Extremophiles*. 17: 301–309.

845 Reis, P.C.J., Martinelli, L.A., Barbosa, F.A.R., 2016. Basal carbon sources and planktonic  
846 food web in a tropical lake: an isotopic approach. *Mar. Freshwater Res.* 68: 429-441.

847 Rochelle-Newall, E., Delille, B., Frankignoulle, M., Gattuso, J.P., Jacquet, S., Riebesell, U.,  
848 Terbruggen, A., Zondervan, I., et al., 2004. Chromophoric dissolved organic matter in  
849 experimental mesocosms maintained under different pCO<sub>2</sub> levels. *Mar. Ecol. Prog. Ser.* 272:  
850 25–31.

851 Roiha, T., Peura, S., Cusson, M., Rautio, M., 2016. Allochthonous carbon is a major  
852 regulator to bacterial growth and community composition in subarctic freshwaters. *Sci. Rep.*  
853 6: 1–12.

854 Sanders, R.W., Cooke, S.L., Fischer, J.M., Fey, S.B., Heinze, A.W., Jeffrey, W.H., A.L.,  
855 Macaluso, Moellert, R.E., et al., 2015. Shifts in microbial food web structure and productivity  
856 after additions of naturally occurring dissolved organic matter: Results from large-scale  
857 lacustrine mesocosms. *Limnol. Oceanogr.* 60: 2130–2144.

858 Sarmiento, H., Morana, C., Gasol, J.M., 2016. Bacterioplankton niche partitioning in the use  
859 of phytoplankton-derived dissolved organic carbon: quantity is more important than quality.  
860 *ISME J.* 10: 2582-2592.

861 Schloss, P.D., Westcott, S.L., Ryabin, T., Hall, J.R., Hartmann, M., Hollister, E.B.,  
862 Lesniewski, R.A., Oakley, B.B., et al., 2009. Introducing mothur: Open-source, platform-  
863 independent, community-supported software for describing and comparing microbial  
864 communities. *Appl. Environ. Microbiol.* 75: 7537–7541.

865 Šimek, K., Kasalický, V., Jezbera, J., Jezberová, J., Hejzlar, J., Hahn, M.W., 2010. Broad  
866 habitat range of the phylogenetically narrow R-BT065 cluster, representing a core group of  
867 the betaproteobacterial genus *limnohabitans*. *Appl. Environ. Microbiol.* 76: 631–639.

868 Smith, H.J., Dieser, M., McKnight, D.M., SanClements, M.D., Foreman, C.M., 2018.  
869 Relationship between dissolved organic matter quality and microbial community composition  
870 across polar glacial environments. *FEMS Microbiol. Ecol.* 94: 1–10.

871 Starr, E.P., Shi, S., Blazewicz, S.J., Probst, A.J., Herman, D.J., Firestone, M.K., Banfield,  
872 J.F., 2018. Stable isotope informed genome-resolved metagenomics reveals that  
873 *Saccharibacteria* utilize microbially-processed plant-derived carbon. *Microbiome* 6: 1–12.

874 Sterner, R.W., Elser, J.J., 2002. *Ecological Stoichiometry: The biology of elements from*  
875 *molecules to the Biosphere*. Princeton University Press, Princeton.

876 Tonetta, D., Staehr, P.A., Obrador, B., Brandão, L.P.M., Brighenti, L.S., Petrucio, M.M.,  
877 Barbosa, F.A.R., Bezerra-Neto, J.F., 2018. Effects of nutrients and organic matter inputs in  
878 the gases CO<sub>2</sub> and O<sub>2</sub>: A mesocosm study in a tropical lake. *Limnologica.* 69: 1–9.

879 Weishaar, J.L., Aiken, G.R., Bergamaschi, B.A., Fram, M.S., Fujii, R., Mopper, K., 2003.  
880 Evaluation of specific ultraviolet absorbance as an indicator of the chemical composition and  
881 reactivity of dissolved organic carbon. *Environ. Sci. Technol.* 37: 4702–4708.

882 Wickham, H., 2016. *ggplot2: elegant graphics for data analysis*. Springer New York.

883 Wiegel, J., Tanner, R., Rainey, F.A., 2006. An introduction to the family Clostridiaceae. In  
884 *The Prokaryotes: a handbook on the biology of bacteria*, 3rd edn, vol. 4, pp. 654–678. Edited  
885 by M. Dworkin, S. Falkow, E. Rosenberg, K. H. Schleifer & E. Stackebrandt. Springer: New  
886 York.

887 Wu, X., Wu, L., Liu, Y., Zhang, P., Li, Q., Zhou, J., Hess, N.J., Hazen, T.C., et al., 2018.  
888 Microbial interactions with dissolved organic matter drive carbon dynamics and community  
889 succession. *Front. Microbiol.* 9: 1–12.

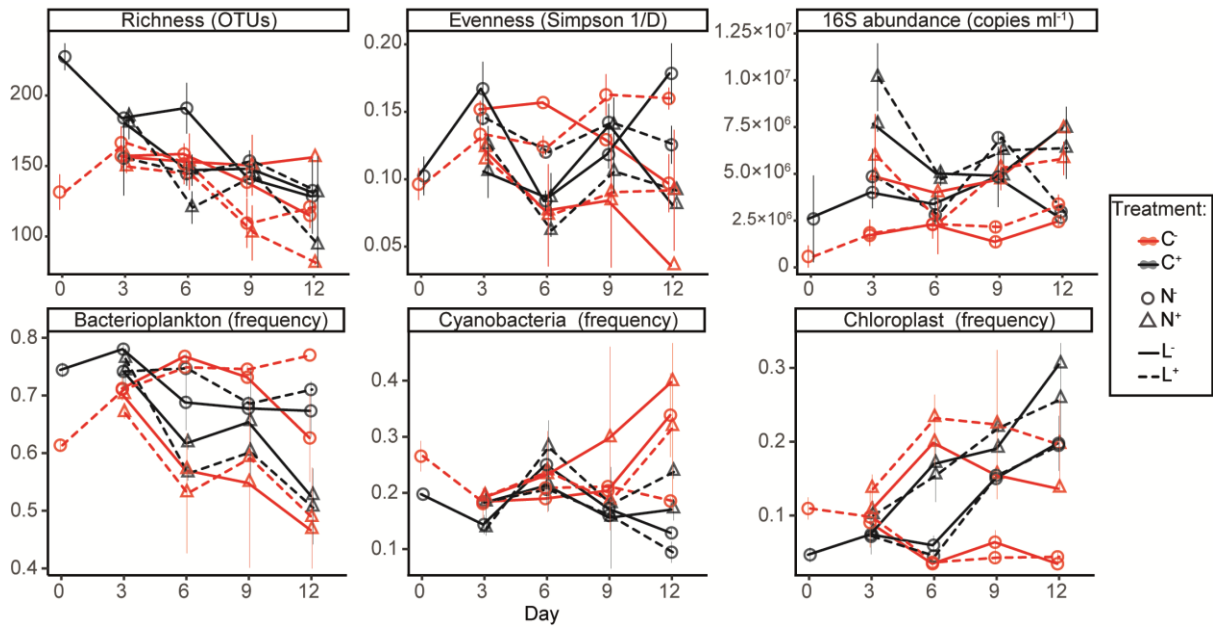
890 Zhang, C., Dang, H., Azam, F., Benner, R., Legendre, L., Passow, U., Polimene, L.,  
891 Robinson, C., et al., 2018. Evolving paradigms in biological carbon cycling in the ocean.  
892 *National Science Review.* 5: 481–499.

893 Zhang, J., Zhang, X., Liu, Y., Xie, S., Liu, Y., 2014. Bacterioplankton communities in a high-  
894 altitude freshwater wetland. *Ann. Microbiol.* 64: 1405–1411.

895 Zhang, Z., Chen, Y., Wang, R., Cai, R., Fu, Y., Jiao, N., 2015. The fate of marine bacterial  
896 exopolysaccharide in natural marine microbial communities. *PLoS One.* 10: 1–16.

897

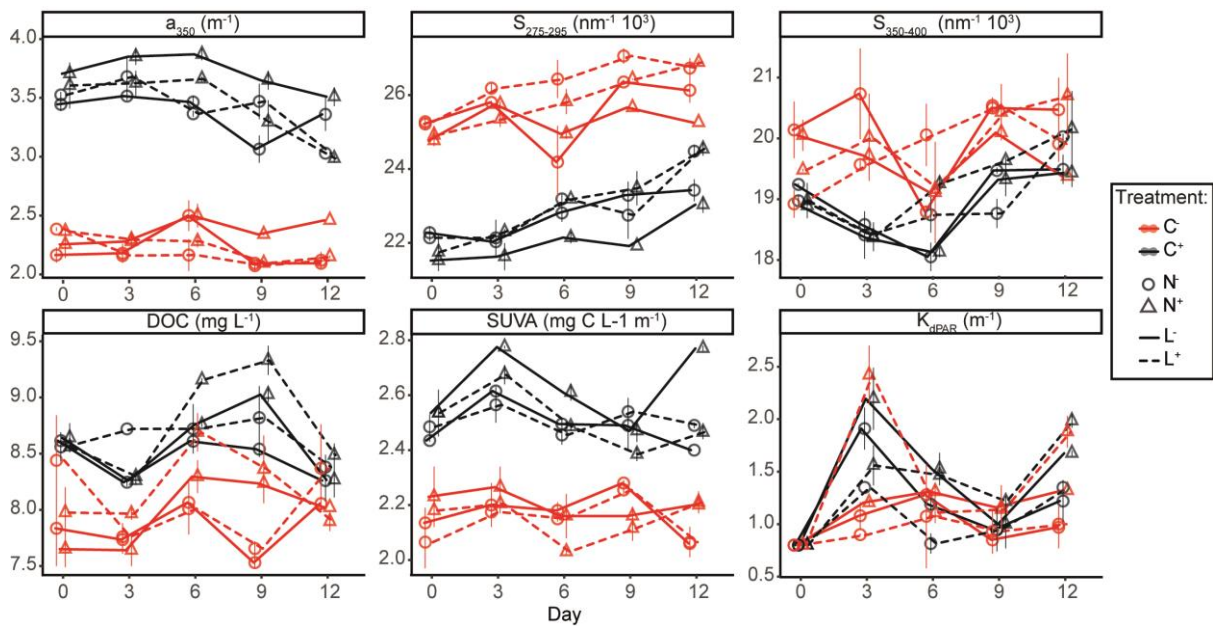
898 **Figures**



899

900 **Figure 1.**

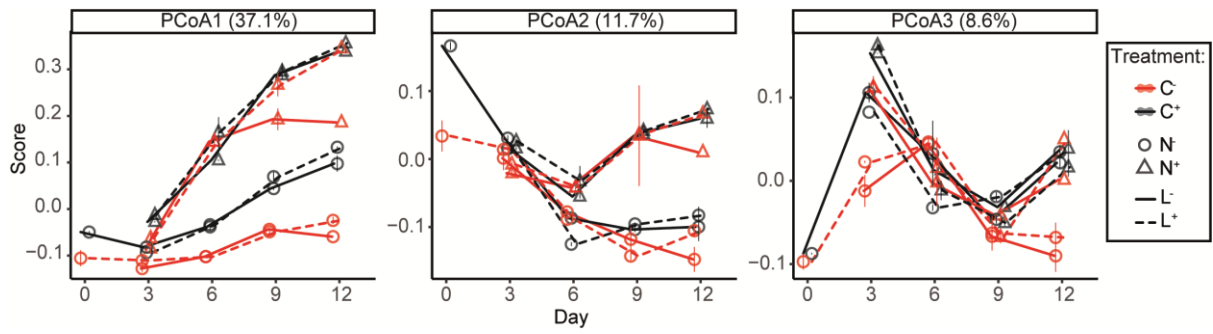
901



902

903 **Figure 2.**

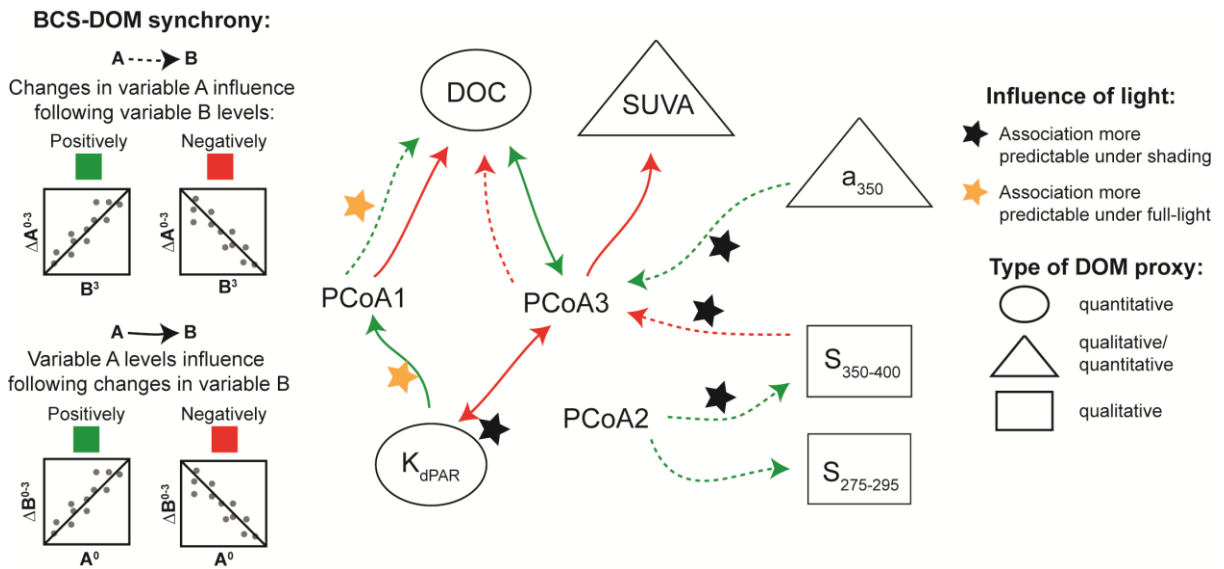
904



905

906 Figure 3.

907

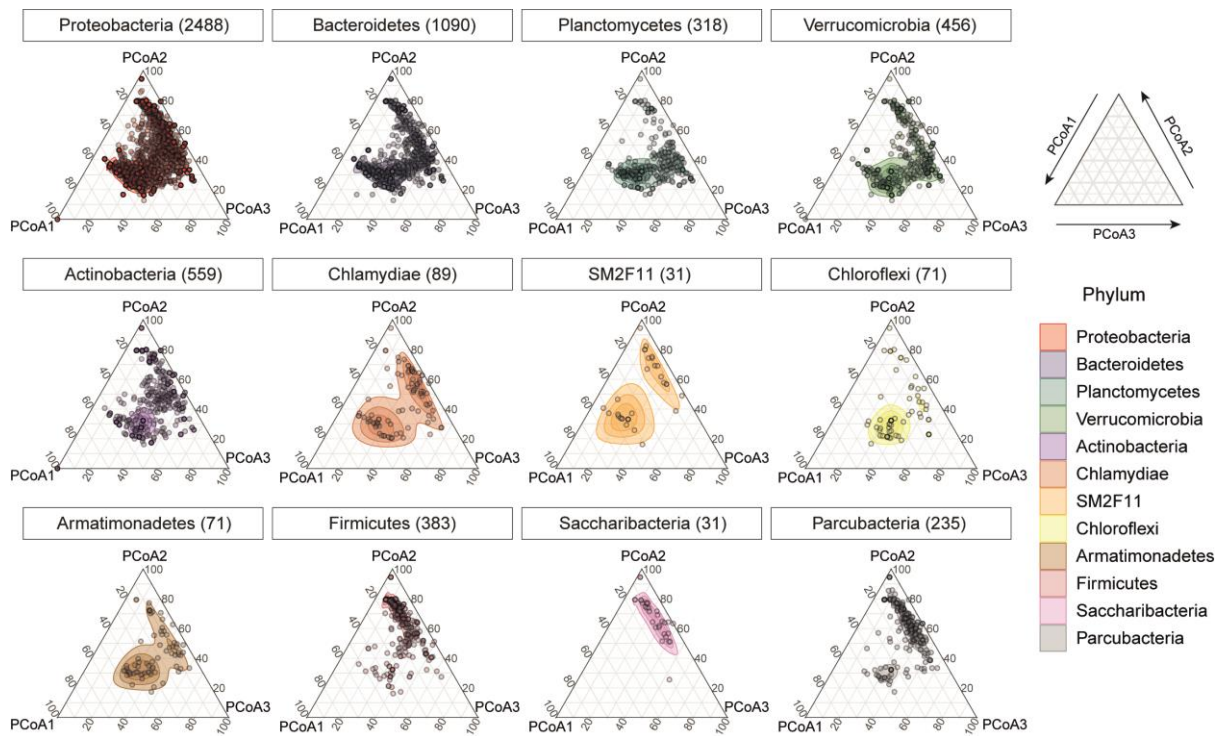


908

909 Figure 4.

910

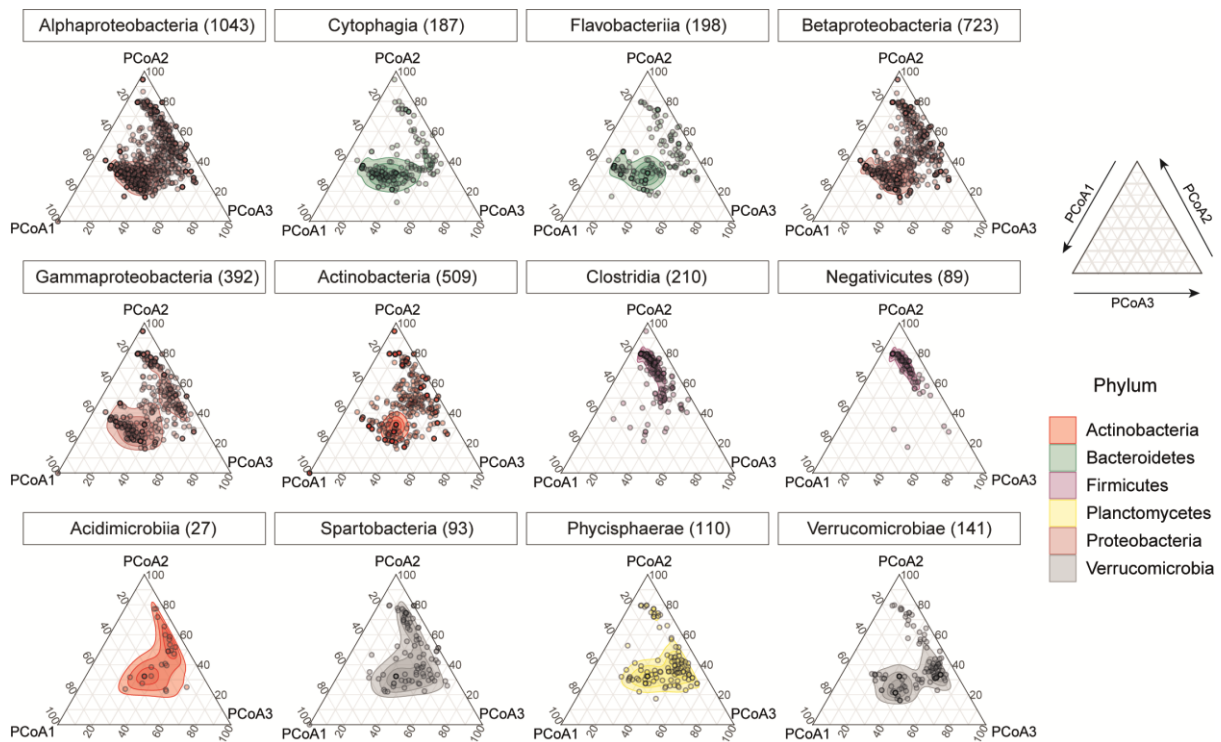




911

912 Figure 5.

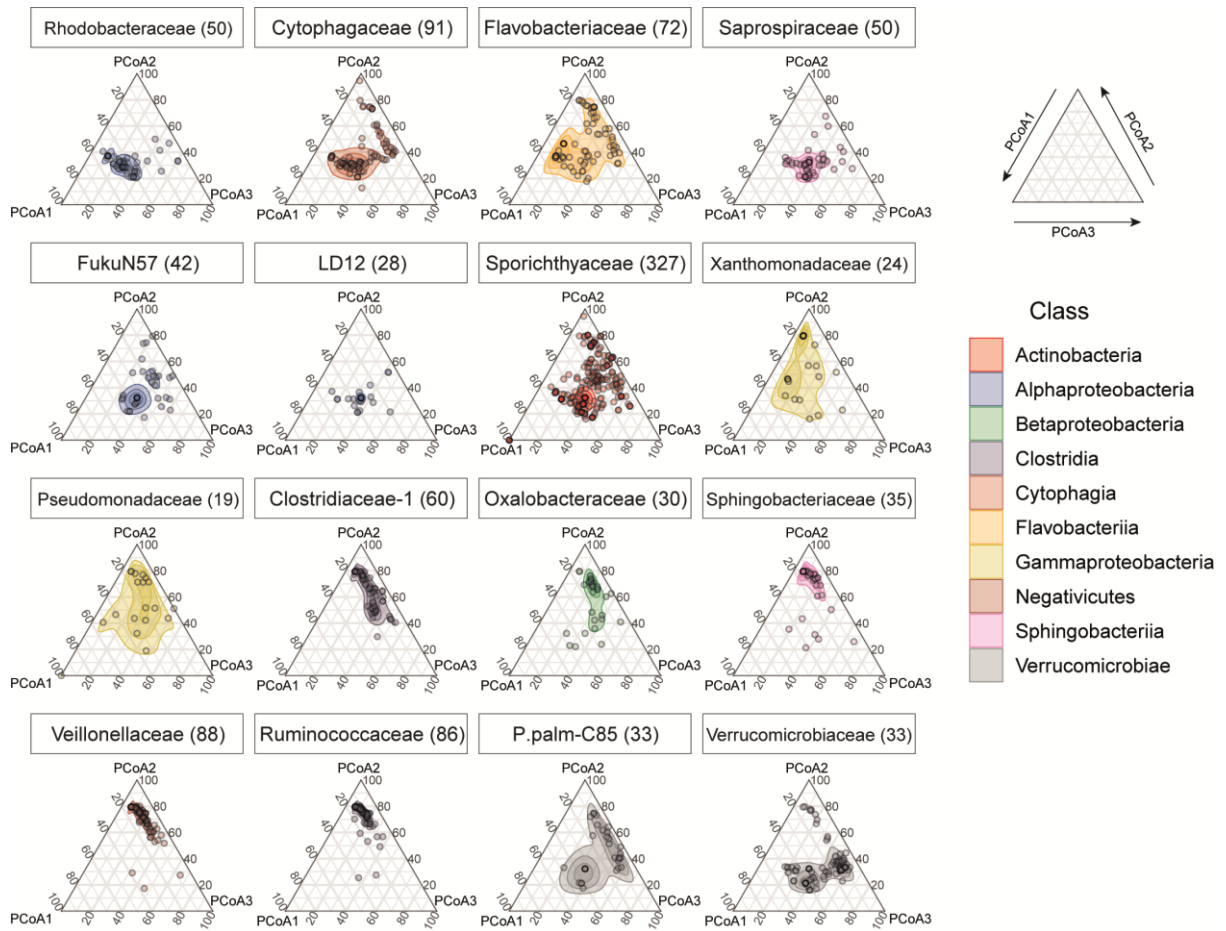
913

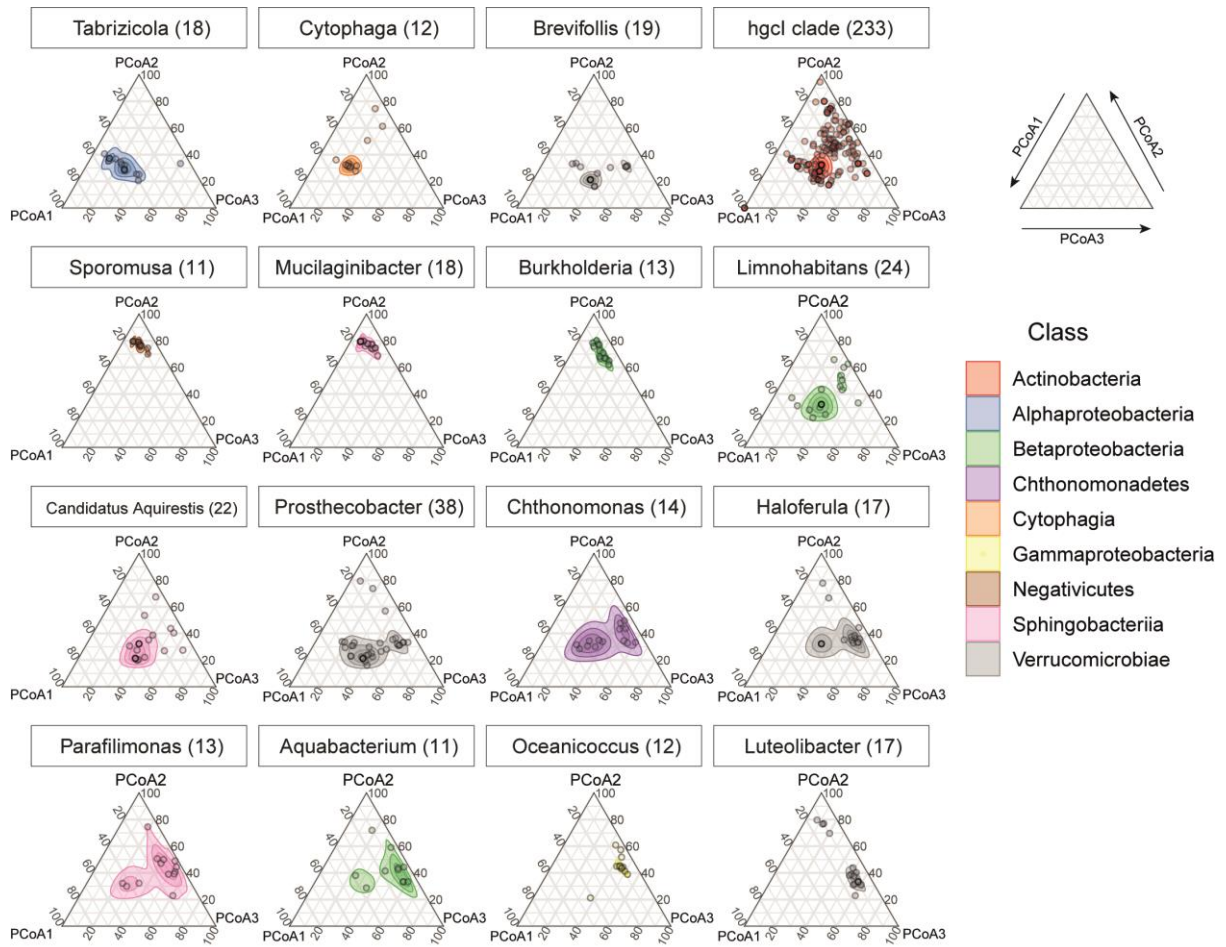


914

915 Figure 6.

916





920

921 Figure 8.

922 **Tables**

923 **Table 1:** Multiple linear regressions results, displaying the effect of the manipulations as mean overall changes and changes per day (indicated  
 924 by the interaction of the manipulation with time) on 16S abundance, bacterioplankton richness and evenness and the relative frequency of  
 925 bacterioplankton, cyanobacteria and chloroplasts.

926

			Allochthonous DOM addition	Nutrient addition	Shading	Combined addition
	adj R <sup>2</sup>	change per day (control)	overall change/ daily change	overall change/ daily change	overall change	overall change
<b>16S abundance</b>	0.48	-	+331.0% [***]/ -19.3% [.]	+291.1% [**]/ -	-	-
<b>Richness</b>	0.55	-1.9% [*]	+25.5% [**]/ -	-	+15.1% [.]	-
<b>Evenness</b>	0.22	-	-	-/ -3.1% [.]	-	-
<b>Bacterioplankton</b>	0.56	-	-	-/ -2.9% [***]	-	-
<b>Cyanobacteria</b>	0.19	-	-/ -5.8% [*]	-/ +5.3% [*]	-	-
<b>Chloroplasts</b>	0.72	-5.0% [.]	-86.0% [**]/ +18.0% [****]	+65.3% [*/] +8.4% [**]	-	-53.4% [*]

927 Non-significant effects are indicated by a dash symbol “-“. 16S abundance accounted for bacterioplankton, cyanobacteria and chloroplasts  
 928 together. The symbols [.] , [\*] , [\*\*] , [\*\*\*] , [\*\*\*\*] indicates the p-value of each regression as marginally significant (0.1-0.05), 0.05-0.01, 0.01-  
 929 10E<sup>-3</sup>, 10E<sup>-3</sup>-10E<sup>-5</sup>, <10E<sup>-5</sup>, respectively.

930 **Table 2:** Multiple linear regressions results, displaying the effect of the manipulations as mean overall changes and changes per day (indicated  
 931 by the interaction of the manipulation with time) on dissolved organic carbon (DOC), aromaticity (SUVA), absorbance at 350 nm ( $a_{350}$ ) and the  
 932 spectral slopes between 275-295nm ( $S_{275-295}$ ) and 350-400nm ( $S_{350-400}$ ).  
 933

		Allochthonous DOM addition		Nutrient addition	Shading	Nutrient addition shaded
	adj R <sup>2</sup>	change per day (control)	overall change/ daily change	overall change/ daily change	overall change/ daily change	overall change
<b>DOC</b>	0.45	-	+8.7% [***]/ -	-	-	-
<b>SUVA</b>	0.79	-	+17.2% [****]/ -	+3.9% [.] / -	-	-
<b>a<sub>350</sub></b>	0.94	-0.96% [**]	+56.5% [****]/ -1.1% [**]	+9.1% [.] / -	-7.7% [.] / -	+9.1% [**]
<b>S<sub>275-295</sub></b>	0.91	+0.2% [.]	-13.3% [****]/ +0.2% [.]	-2.2% [.] / -	- / -0.3% [**]	-
<b>S<sub>350-400</sub></b>	0.42	-	-6.5% [**]/ -	-	+3.7% [.] / -0.4% [.]	-2.6% [.]

934 Non-significant effects are indicated by a dash symbol “-“. The symbols [.] , [\*], [\*\*], [\*\*\*], [\*\*\*\*] indicates the p-value of each regression as  
 935 marginally significant (0.1-0.05), 0.05-0.01, 0.01-10E<sup>-3</sup>, 10E<sup>-3</sup>-10E<sup>-5</sup>, <10E<sup>-5</sup>, respectively.  
 936

937 **Table 3:** Multiple linear regressions results, displaying the effect of the manipulations as mean overall changes and changes per day (indicated  
 938 by the interaction of the manipulation with time) on the main principal coordinates PCoA1, PCoA2 and PCoA3.  
 939

				Allochthonous addition	DOM	Nutrient addition	Shading	Combined addition
	% of community variance	adj R <sup>2</sup>	change per day (control)	overall change/ daily change		overall change/ daily change	daily change	overall change
<b>PCoA1</b>	37.1%	0.93	+10.5% [*]	+67.4% [.] / +11.7% [**]		- / +42.4% [****]	-	-83.9% [**]
<b>PCoA2</b>	11.7%	0.68	-7.3% [****]	-		-41.0% [***] / +9.2% [****]	-2.5% [.]	-
<b>PCoA3</b>	8.6%	0.25	-	-		+75.3% [***] / -6.8% [**]	-	-

940 The percentage of variance explained by each axis is also displayed. Non-significant effects are indicated by a dash symbol “-“. The symbols [.] ,  
 941 [\*], [\*\*], [\*\*\*], [\*\*\*\*] indicates the p-value of each regression as marginally significant (0.1-0.05), 0.05-0.01, 0.01-10E<sup>-3</sup>, 10E<sup>-3</sup>-10E<sup>-5</sup>, <10E<sup>-5</sup>,  
 942 respectively.  
 943

944 **Table 4:** Effect of BCS on DOM. Results of the of linear regressions tested between DOM proxies and BCS, which was evaluated as changes in  
 945 scores of the three main PCoA's axes within three-day intervals. The results show significant associations ( $p$ -value < 0.05,  $R^2$  > 0.2) about  
 946 changes in BCS that determine DOM fate ( $\Delta\text{PCoA}^{0-3} \sim \text{DOM}^3$ ) and changes in DOM pool that are determined by a previous community  
 947 ( $\Delta\text{DOM}^{0-3} \sim \text{PCoA}^0$ ).  
 948

Changes in BCS determine DOM						BCS determines changes in DOM					
<b>All treatments + control</b>											
$\Delta\text{PCoA}^{0-3}$ (y)	$\text{DOM}^3$ (x)	<i>intercept</i>	<i>coef.</i>	$R^2$	<i>p-value</i>	$\Delta\text{DOM}^{0-3}$ (y)	$\text{PCoA}^0$ (x)	<i>intercept</i>	<i>coef.</i>	$R^2$	<i>p-value</i>
<b>PCoA1</b>	<b>DOC</b>	-0.570	0.077	0.273	1.65E-04	<b>DOC</b>	<b>PCoA3</b>	-0.022	3.783	0.288	1.02E-04
						<b>SUVA</b>	<b>PCoA3</b>	-0.003	-0.845	0.217	0.001
<b>Only treatments</b>											
$\Delta\text{PCoA}^{0-3}$ (y)	$\text{DOM}^3$ (x)	<i>intercept</i>	<i>coef.</i>	$R^2$	<i>p-value</i>	$\Delta\text{DOM}^{0-3}$ (y)	$\text{PCoA}^0$ (x)	<i>intercept</i>	<i>coef.</i>	$R^2$	<i>p-value</i>
<b>PCoA2</b>	<b>S<sub>275-295</sub></b>	-0.546	0.022	0.213	0.007	<b>DOC</b>	<b>PCoA1</b>	0.164	-2.757	0.442	2.47E-05
<b>PCoA2</b>	<b>S<sub>350-400</sub></b>	-1.152	0.059	0.385	1.17E-04	<b>DOC</b>	<b>PCoA3</b>	-0.114	5.290	0.657	1.07E-08
<b>PCoA3</b>	<b>DOC</b>	1.073	-0.128	0.244	0.003	<b>SUVA</b>	<b>PCoA3</b>	0.026	-1.345	0.589	3.02E-07
<b>PCoA3</b>	<b>K<sub>dPAR</sub></b>	-0.208	0.139	0.219	0.006						

949  
950

951 **Table 5:** Effect of DOM on BCS. Results of the of linear regressions tested between DOM proxies and BCS, which was evaluated as changes in  
 952 scores of the three main PCoA's axes within three-day intervals. The results show significant associations ( $p$ -value < 0.05,  $R^2 > 0.2$ ) about  
 953 changes in DOM that determine BCS fate ( $\Delta\text{DOM}^{0-3} \sim \text{PCoA}^3$ ) and changes in BCS that are determined by a previous DOM pool ( $\Delta\text{PCoA}^{0-3} \sim$   
 954  $\text{DOM}^0$ ).  
 955

Changes in DOM determine BCS						DOM determines changes in BCS					
<b>All treatments + control</b>											
						$\Delta\text{PCoA}^{0-3}$ (y)	$\text{DOM}^0$ (x)	<i>intercept</i>	<i>coef.</i>	$R^2$	<i>p-value</i>
						PCoA1	$K_{d\text{PAR}}$	-0.035	0.089	0.344	1.82E-05
						PCoA3	$K_{d\text{PAR}}$	0.120	-0.111	0.299	8.45E-05
<b>Only treatments</b>											
$\Delta\text{DOM}^{0-3}$ (y)	$\text{PCoA}^3$ (x)	<i>intercept</i>	<i>coef.</i>	$R^2$	<i>p-value</i>	$\Delta\text{PCoA}^{0-3}$ (y)	$\text{DOM}^0$ (x)	<i>intercept</i>	<i>coef.</i>	$R^2$	<i>p-value</i>
$S_{350-400}$	PCoA3	0.276	-10.168	0.286	0.001	PCoA1	$K_{d\text{PAR}}$	0.002	0.071	0.251	0.003
						PCoA3	DOC	-0.932	0.106	0.207	0.008
						PCoA3	$K_{d\text{PAR}}$	0.146	-0.125	0.372	2.08E-04

956  
 957